



# Impact of fossil and non-fossil fuel sources on the molecular compositions of water-soluble humic-like substances in PM<sub>2.5</sub> at a suburban site of Yangtze River Delta, China

Mengying Bao<sup>1,2,3</sup>, Yan-Lin Zhang<sup>1,2</sup>, Fang Cao<sup>1,2</sup>, Yihang Hong<sup>1,2</sup>, Yu-Chi Lin<sup>1,2</sup>, Mingyuan Yu<sup>1,2</sup>, Hongxing Jiang<sup>4,5</sup>, Zhineng Cheng<sup>4,5</sup>, Rongshuang Xu<sup>1,2</sup>, and Xiaoying Yang<sup>1,2</sup>

<sup>1</sup>School of Applied Meteorology, Nanjing University of Information Science and Technology, Nanjing 210044, China

<sup>2</sup>Atmospheric Environment Center, Joint Laboratory for International Cooperation on Climate and Environmental Change, Ministry of Education (ILCEC), Nanjing University of Information Science and Technology, Nanjing 210044, China

<sup>3</sup>Huzhou Meteorological Administration, Huzhou 313300, China

<sup>4</sup>State Key Laboratory of Organic Geochemistry and Guangdong province Key Laboratory of Environmental Protection and Resources Utilization, Guangzhou Institute of Geochemistry, Chinese Academy of Sciences, Guangzhou 510640, China

<sup>5</sup>CAS Center for Excellence in Deep Earth Science, Guangzhou Institute of Geochemistry, Chinese Academy of Sciences, Guangzhou 510640, China

**Correspondence:** Yan-Lin Zhang (dryanlinzhang@outlook.com)

Received: 12 September 2022 – Discussion started: 4 October 2022

Revised: 8 June 2023 – Accepted: 9 June 2023 – Published: 25 July 2023

**Abstract.** Atmospheric humic-like substances (HULIS) affect the global radiation balance due to their strong light absorption at the ultraviolet wavelength. The potential sources and molecular compositions of water-soluble HULIS at a suburban site in the Yangtze River Delta from 2017 to 2018 were discussed, based on the results of the radiocarbon (<sup>14</sup>C) analysis and combining the Fourier transform ion cyclotron resonance mass spectrometry (FT-ICR-MS) technique in this study. The <sup>14</sup>C results showed that the averaged non-fossil-fuel source contributions to HULIS were 39 ± 8 % and 36 ± 6 % in summer and winter, respectively, indicating significant contributions from fossil fuel sources to HULIS. The Van Krevelen diagrams obtained from the FT-ICR-MS results showed that the proportions of tannin-like and carbohydrate-like groups were higher in summer, suggesting significant contribution of HULIS from biogenic secondary organic aerosols (SOAs). The higher proportions of condensed aromatic structures in winter suggested increasing anthropogenic emissions. Molecular composition analysis on the CHO, CHON, CHOS, and CHONS subgroups showed relatively higher intensities of high O-containing macromolecular oligomers in the CHO compounds in summer, further indicating stronger biogenic SOA formation in summer. High-intensity phenolic substances and flavonoids, which were related to biomass burning and polycyclic aromatic hydrocarbon (PAH) derivatives indicating fossil fuel combustion emissions, were found in winter CHO compounds. Besides, two high-intensity CHO compounds containing condensed aromatic ring structures (C<sub>9</sub>H<sub>6</sub>O<sub>7</sub> and C<sub>10</sub>H<sub>5</sub>O<sub>8</sub>) identified in the summer and winter samples were similar to those from off-road engine samples, indicating that traffic emissions were one of the important fossil fuel sources of HULIS at the study site. The CHON compounds were mainly composed of nitro compounds or organonitrates with significantly higher intensities in winter, which were associated with biomass burning emissions, in addition to the enhanced formation of organonitrates due to high NO<sub>x</sub> in winter. However, the high-intensity CHON molecular formulas in summer were referring to N-heterocyclic aromatic compounds, which were produced from the

atmospheric secondary processes involving reduced N species (e.g., ammonium). The S-containing compounds were mainly composed of organosulfates (OSs) derived from biogenic precursors, namely long-chain alkane and aromatic hydrocarbon, which illustrate the mixed sources of HULIS. Generally, different policies need to be considered for each season due to the different seasonal sources (i.e., biogenic emissions in summer and biomass burning in winter for non-fossil-fuel sources, traffic emissions and anthropogenic SOA formation in both seasons, and additional coal combustion in winter). Measures to control emissions from motor vehicles and industrial processes need to be considered in summer. Additional control measures on coal power plants and biomass burning should be applied in winter. These findings add to our understanding of the interaction between the sources and the molecular compositions of atmospheric HULIS.

## 1 Introduction

Atmospheric humic-like substances (HULIS) have been observed worldwide and can be produced from the primary combustion of biomass, fossil fuels, and various secondary processes, such as the photochemical processes of volatile organic compounds (VOCs) and heterogeneous reactions of organic aerosols in the atmosphere (Kuang et al., 2015; Li et al., 2019; Ma et al., 2018; Sun et al., 2021). As they are an important component of brown carbon (BrC) aerosols, HULIS species have been widely reported to have a great impact on the global radiative budget, contributing to 20%–40% of the direct radiative forcing caused by light-absorbing aerosols, due to its light absorption at the ultraviolet wavelength (Chung et al., 2012; Zhang et al., 2017; A. Zhang et al., 2020; X. Wang et al., 2018). HULIS are a highly complex mixture of polar organic compounds composed of aromatic and hydrophobic aliphatic structures containing carboxyl, carbonyl, and hydroxyl function groups (Zheng et al., 2013; Graber and Rudich, 2006; T. Zhang et al., 2022a, b). During the atmospheric secondary oxidation processes, the substitutions of hydrophilic functional groups increased the aerosol hygroscopicity (Huo et al., 2021; Jiang et al., 2020). Polycarboxylic acids in HULIS are surface-active and play an important role in the cloud condensation nuclei (CCN) activity (Tsui and McNeill, 2018). N-based compounds can promote the generation of atmospheric reactive oxygen species (ROS), which have a great impact on human health (Y. Wang et al., 2017; De Haan et al., 2018; Song et al., 2022). Identifying the molecular compositions of HULIS is a challenge due to complex mixtures contained in HULIS but can help give a better understanding of the processes involving organic compounds in the atmosphere (Noziere et al., 2015; Laskin et al., 2018).

The Fourier transform ion cyclotron resonance mass spectrometry (FT-ICR-MS) coupled with electrospray ionization (ESI) ion source has been widely used in identifying the chemical structure of HULIS, providing high mass accuracy and determining molecular formulas from mixed compounds (Chen et al., 2016; Y. Wang et al., 2019; Lin et al., 2012a; Jiang et al., 2020). Typical molecular formulas composed of C, H, and O atoms in HULIS were observed

as being abundant in carboxylic acids, lignin-derived products, and polycyclic aromatic hydrocarbons (PAHs) or their derivatives (Lin et al., 2012a; Sun et al., 2021; Jiang et al., 2020; Huo et al., 2021; Song et al., 2018). In addition, the HULIS formation of N- and S-containing precursors was also widely detected (Lin et al., 2012b; Sun et al., 2021; Song et al., 2018). The N-containing compounds such as nitroaromatics were important chromophores in HULIS in aged biomass burning organic aerosols (BBOAs), and in ambient aerosols influenced by biomass burning (BB), while reduced N compounds such as N-heterocyclic aromatic compounds were found to be important chromophores in fresh BBOAs (Y. Wang et al., 2019; Song et al., 2022; Jiang et al., 2020; Y. Wang et al., 2017). Recent laboratory simulation experiments showed that the photooxidation of various anthropogenic VOCs (e.g., naphthalene, benzene, toluene, and ethylbenzene) would be promoted under high  $\text{NO}_x$  conditions, thus producing strongly light-absorbing nitroaromatics (Yang et al., 2022; Aiona et al., 2018; Siemens et al., 2022; Xie et al., 2017). Otherwise, the nighttime oxidation of biogenic or anthropogenic VOCs, such as benzene/toluene, isoprenes ( $\text{C}_5\text{H}_8$ ), and monoterpenes ( $\text{C}_{10}\text{H}_{16}$ ) by  $\text{NO}_3$  radicals lead to the formation of substantial organonitrates, where the VOC oxidation is strongly affected by  $\text{NO}_x$  (He et al., 2021; Shen et al., 2021; Wang et al., 2020; Zheng et al., 2021).

The organosulfates (OSs) and nitrooxy organosulfates (nitrooxy-OSs) have also been found to exist widely in HULIS in different atmospheric environments (Lin et al., 2012b, a; Sun et al., 2021). Field study and laboratory smog chamber experiments have confirmed that OSs and nitrooxy-OSs in the atmosphere mainly come from the  $\text{O}_3$ , OH, or  $\text{NO}_3$  oxidation of biogenic VOCs such as isoprene,  $\alpha/\beta$ -pinene, and aromatic hydrocarbon in the presence of  $\text{H}_2\text{SO}_4/\text{SO}_2$  (Surratt et al., 2008; Glasius et al., 2021; Yang et al., 2020; Lin et al., 2012b; Huang et al., 2020). Coal combustions were found to be important sources of the aromatic OSs and nitrooxy-OSs in HULIS (Song et al., 2018). Besides, the long-chain alkanes were found to be an important precursor of OSs in atmospheric aerosol samples from urban areas, which was related to vehicle emissions (K. Wang et al., 2019; Tao et al., 2014).

Nanjing is one of the main cities in the Yangtze River Delta (YRD), which is one of the most developed areas in China. Organic matter can account for 20%–40% of PM<sub>2.5</sub> in the YRD area due to the impact of complicated sources, especially anthropogenic emissions (J. Wang et al., 2017, 2016). Studies have reported that BrC is an important contributor to aerosol light absorption in Nanjing, and it has exhibited obvious seasonal variations, with peaks in wintertime, owing to emissions from biomass burning, fossil fuel combustion, and secondary formation (Chen et al., 2018; Cui et al., 2021; Xie et al., 2020; J. Wang et al., 2018). Recently, research works on the field observation of nitrated aromatic compounds (NACs) were conducted to explore the light absorption contributions of NACs to BrC and help to better understand the links between the optical properties and molecular compositions of BrC (Gu et al., 2022; Cao et al., 2023). However, as far as we know, understanding of the sources of atmospheric HULIS at molecular levels was still limited. In this work, the molecular compositions of water-soluble HULIS isolated from PM<sub>2.5</sub> samples collected in summertime and wintertime from 2017 to 2018 at Nanjing, China, were investigated by combining the FT-ICR-MS and radiocarbon (<sup>14</sup>C) analysis. We aim to obtain the molecular characteristic differences in the water-soluble HULIS in summertime and wintertime and to obtain a better understanding of the influence of different sources on the molecular compositions of HULIS.

## 2 Materials and methods

### 2.1 Sample collection

The 24 h PM<sub>2.5</sub> samples were collected on the roof of the Wende building, which is about 21 m a.g.l. (above ground level) at the Nanjing University of Information Science and Technology (32.2° N, 118.7° E), using a high-volume sampler (KC-1000, Qingdao Laoshan Electronic Instrument Factory Co., Ltd, China) at a flow rate of 300 L min<sup>-1</sup>. The study site was located in the northern suburban area of Nanjing, adjacent to the China National Highway 205 (G205) and surrounded by an industrial park and residential area. Generally, the study site was affected by human activity, industrial emissions, and traffic emissions. The sample collection was conducted in summer from 12 to 26 August 2017 and in winter from 31 December 2017 to 31 January 2018. A heavy haze event occurred from 31 December 2017 to 3 January 2018; thus, the sample frequency was adjusted to 2 h in the daytime and 8 h during the nighttime. Field blank filters were performed before and after sample collection for each season. More details about the sample collection can be found in previous research reported by Bao et al. (2022). The air pollutant data, including PM<sub>2.5</sub>, SO<sub>2</sub>, and NO<sub>2</sub>, were provided by China National Environmental Monitoring Centre. In total, 12 samples were selected for further chemical anal-

ysis, and the details about the sample selection are described in Sect. 3.1 in this study.

### 2.2 Chemical analysis

The solid-phase extraction (SPE) cartridge (Oasis HLB; 30 µm; 60 mg per cartridge; Waters Corporation, USA) was performed to isolate the water-soluble HULIS in this study. Briefly, the prepared water extracts first passed through the preconditioned HLB cartridge, then the retained HULIS on the HLB cartridge were eluted with 2% (v/v) ammonia/methanol and evaporated to dryness under a gentle stream of nitrogen gas, and finally redissolved in ultrapure water for the measurement. The carbon fraction in HULIS (HULIS-C) were determined using a total carbon analyzer (TOC-VCPH; Shimadzu Corporation, Japan) with a standard deviation of the reproducibility test of less than 3.5% and a detection limit of 0.14 µg C m<sup>-3</sup>. More details about the HULIS isolation and measurement have been described in Bao et al. (2022).

The mass concentrations of the water-soluble ions, including NO<sub>3</sub><sup>-</sup>, NH<sub>4</sub><sup>+</sup>, and SO<sub>4</sub><sup>2-</sup>, were measured using an ion chromatography (Dionex ICS-5000+; Thermo Fisher Scientific, USA) separated on an AS11 column (4 × 250 mm; Dionex ICS-5000+; Thermo Fisher Scientific, USA) for anions and a CS12A column (4 × 250 mm; Dionex ICS-5000+; Thermo Fisher Scientific, USA) for cations, respectively. Potassium hydrate (KOH) and methane sulfuric acid (MSA) were used as the gradient eluent for anion and cation determination, respectively. The levoglucosan concentrations were analyzed using the same ion chromatograph equipped with a CarboPac MA1 analytical column (4 × 250 mm; Dionex ICS-5000+; Thermo Fisher Scientific, USA) and an electrochemical detector. Sodium hydroxide (NaOH) was used as the gradient eluent for levoglucosan determination. All data were blank-corrected in this study. More details of the methods have been described previously (Liu et al., 2019).

### 2.3 Radiocarbon analysis

For the radiocarbon measurement of the HULIS samples, the organic solvents were firstly evaporated under a gentle flow of ultrapure N<sub>2</sub> for 30–40 min in tin cups. After that, the tin cups were wrapped into balls and more than 50 µg of carbon from the HULIS samples was combusted into CO<sub>2</sub> using an elemental analyzer (EA, model vario EL cube; Elementar Analysensysteme GmbH, Germany), then reduced into graphite targets for <sup>14</sup>C determination at the State Key Laboratory of Organic Geochemistry, Guangzhou Institute of Geochemistry, Guangzhou, China (Jiang et al., 2020). Detailed descriptions of the <sup>14</sup>C data processing can be found in a previous study (Mo et al., 2018). Briefly, the <sup>14</sup>C values were expressed as the modern carbon (*f<sub>m</sub>*) fraction after correcting for the δ<sup>13</sup>C fractionation. The *f<sub>m</sub>* was converted into a non-fossil-fuel carbon (*f<sub>nf</sub>*) fraction with the correction

factor of  $1.06 \pm 0.07$ , based on the long-term time series of  $^{14}\text{CO}_2$  sampled at the background station in this study (Levin et al., 2013; Levin and Kromer, 2004).  $^{14}\text{C}$  analysis of the oxalic acid standard (IAEA-C7) was conducted in this study (Xu et al., 2021). No field blank correction was performed for the carbon isotope analysis, since the carbon content in the field blanks was negligible.

## 2.4 High-resolution FT-ICR-MS analysis

The ultrahigh-resolution mass spectra of the HULIS samples were obtained through a solarix XR FT-ICR-MS (Bruker Daltonics GmbH, Bremen, Germany) equipped with a 9.4 T superconducting magnet (Gamry Instruments, Warminster, PA, USA) and a ParaCell analyzer cell (Bruker Daltonics GmbH, Bremen, Germany) in the negative ESI mode. The detection mass range was set as  $m/z$  150 to 800, and the ion accumulation time was set as 0.65 s. A total of 100 continuous  $4 \times 10^6$  transient data points were superposed to enhance the signal-to-noise ratio and dynamic range. The mass spectrum was externally calibrated with a standard solution of arginine, and internal recalibration was performed using typical  $\text{O}_6\text{S}_1$  chemical species in DataAnalysis 4.4 software (Bruker Daltonics GmbH, Bremen, Germany; Mo et al., 2018; Tang et al., 2020; Jiang et al., 2020). Field blank filters were analyzed in the same way as the samples, and all the sample data were blank-corrected. More details about the data processing can be found in Sect. S1 in the Supplement.

## 3 Results and discussion

### 3.1 General temporal characteristics during the sampling periods

Figure 1 displays the temporal variations in the non-fossil-fuel contributions to HULIS-C, the mass concentrations of HULIS-C, levoglucosan,  $\text{NO}_3^-$ ,  $\text{SO}_4^{2-}$ ,  $\text{NH}_4^+$ ,  $\text{SO}_2$ ,  $\text{NO}_2$ , and  $\text{PM}_{2.5}$ , as well as the relative humidity and temperature during the study periods corresponding to the 12 samples. The 12 samples were named as S1–S6 (summer) and W1–W6 (winter) and in chronological order, corresponding to the six samples in summer and winter, respectively in this study. The averaged mass concentrations of  $\text{PM}_{2.5}$  in summer and winter during the selected periods were  $21.05 \pm 8.05$  and  $445.67 \pm 275.00 \mu\text{g m}^{-3}$ , respectively, indicating the serious pollution levels in winter. The daily  $\text{PM}_{2.5}$  mass concentrations in summer were all below the daily averaged Chinese National Ambient Air Quality Standards (NAAQS) of  $35 \mu\text{g m}^{-3}$ , while the daily  $\text{PM}_{2.5}$  mass concentrations in winter all exceeded the daily averaged NAAQS of  $35 \mu\text{g m}^{-3}$ , of which the  $\text{PM}_{2.5}$  mass concentrations of W1–W3 and W6 exceeded  $200 \mu\text{g m}^{-3}$ . The averaged mass concentrations of HULIS in summer and winter during the selected periods were  $1.83 \pm 0.27$  and  $4.52 \pm 2.29 \mu\text{g m}^{-3}$ , respectively. Compared with those measured in other cities in China in sum-

mer, the average HULIS concentration in Nanjing in summer was comparable with those measured in Guangzhou of  $1.70 \mu\text{g m}^{-3}$  (Fan et al., 2016), Shanghai of  $1.61 \mu\text{g m}^{-3}$  (Zhao et al., 2016), and Xi'an of  $1.50 \mu\text{g m}^{-3}$  (T. Zhang et al., 2020). Compared with those samples measured in winter in other cities, our result was comparable with those in Xi'an of  $4.50 \mu\text{g m}^{-3}$  (T. Zhang et al., 2020), a little lower than those in the megacity of Shanghai of  $5.31 \mu\text{g m}^{-3}$  (Zhao et al., 2016), and higher than those in the southern coastal city of Guangzhou of  $3.60 \mu\text{g m}^{-3}$  (Fan et al., 2016).

As shown in Fig. 1, the mass concentrations of HULIS-C, levoglucosan, water-soluble secondary inorganic aerosols (SIAs), and air pollutants showed similar trends in winter, suggesting the influence of BB and anthropogenic emissions in winter (G. Wu et al., 2019). The radiocarbon analysis results showed that the  $f_{\text{nf}}$  of HULIS-C ranged from 30 % to 50 %, with an average contribution of  $39 \pm 8$  % in summer, and ranged from 32 % to 48 %, with an average contribution of  $36 \pm 6$  % in winter, indicating the significant contributions from fossil fuel sources to HULIS at the study site. The 48 h back trajectories (Fig. S1 in the Supplement) showed that the study site was affected by the polluted air masses mainly from the northern cities in winter, suggesting that there are coal combustion contributions to HULIS in winter (Ma et al., 2018; Sun et al., 2021). In addition, significant increases in the levoglucosan and HULIS-C mass concentrations were found from 31 December 2017 to 1 January 2018, corresponding to the W1–W3 samples, and the maximum values of the levoglucosan and HULIS-C mass concentrations were  $552.79 \text{ ng m}^{-3}$  and  $7.40 \mu\text{g m}^{-3}$ , respectively, indicating the BB impact during these periods. In summer, the study site was affected by both regional transport from the nearby cities to the north and west of Nanjing and the Donghai sea. The anthropogenic emissions from the neighboring cities might cause the anthropogenic SOA formation, i.e., secondary N-containing and S-containing compounds with aromatic structures during the atmospheric transport processes, which is discussed in detail in Sect. 3.4 in this study.

### 3.2 Mass spectra and molecular formula assignments

Figures S2 and S3 in the Supplement show the negative ion ESI FT-ICR mass spectra of HULIS in summer and winter, respectively. The molecular formulas listed are some of the top 10 molecular formulas. Thousands of peaks are present in the spectra in the range from  $m/z$  150 to  $m/z$  600, and the most intense ion peaks are those in the range  $m/z$  200–400 in summer and  $m/z$  150–350 in winter. Our results are similar to those found for the ultrahigh-resolution mass spectra of water-soluble organic compounds in particles produced from BB, coal combustion, and vehicle exhaust emissions, in addition to ambient aerosols and cloud water samples, within a reasonable range (Tang et al., 2020; Sun et al., 2021; Song et al., 2018, 2019; Bianco et al., 2018). In this study, the assigned molecular formulas were classified into the following



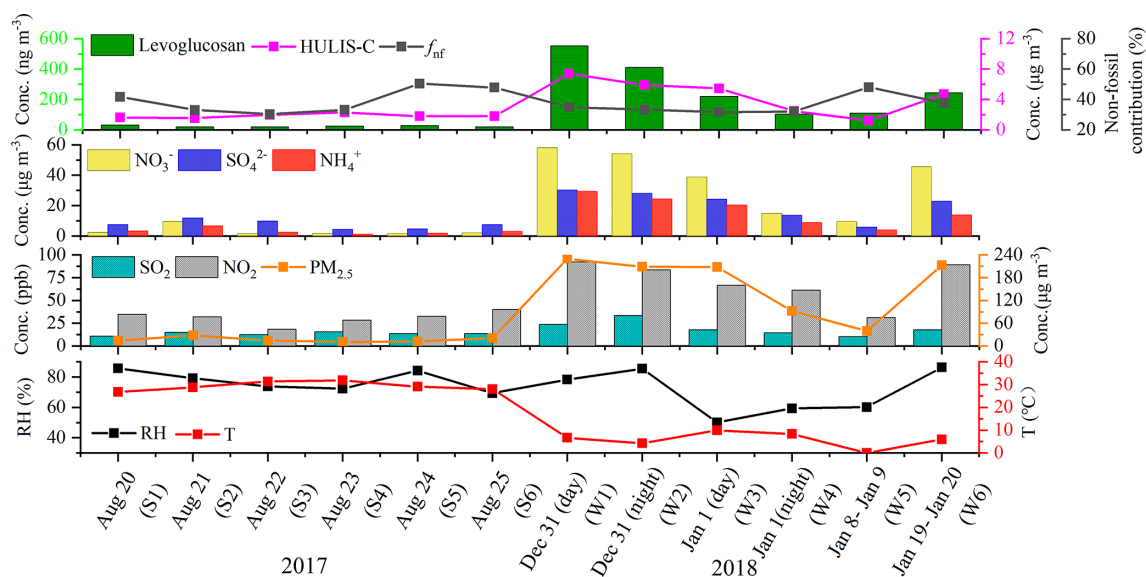


**Figure 1.** Time series of non-fossil contributions to HULIS-C, the mass concentrations of HULIS-C, levoglucosan,  $\text{NO}_3^-$ ,  $\text{SO}_4^{2-}$ ,  $\text{NH}_4^+$ ,  $\text{SO}_2$ ,  $\text{NO}_2$ ,  $\text{PM}_{2.5}$ , relative humidity, and temperature during the study periods.

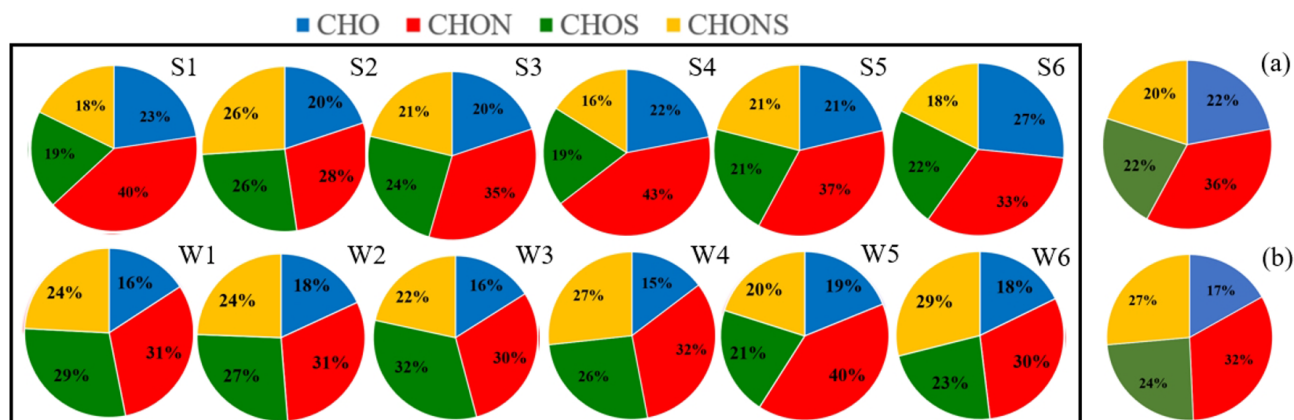


**Figure 2.** Pie graph of the number percentages of each elemental formula group for the 12 samples plotted in the box and the average percentages for each elemental formula group for the summer samples (a) and winter samples (b), respectively.

four main subgroups based on their elemental compositions: CHO compounds containing only C, H, and O; CHON compounds containing C, H, O, and N; CHOS compounds containing C, H, O, and S; and CHONS compounds containing C, H, O, N, and S). As shown in Fig. 2, the proportions of the four subgroups accounted for the overall formulas as follows: CHO (20%–27%), CHON (28%–43%), CHOS (19%–26%), and CHONS (16%–26%) in summer, respectively, and CHO (15%–19%), CHON (30%–40%), CHOS (21%–32%), and CHONS (20%–29%) in winter, respectively. The average proportions of the CHO, CHON, CHOS, and CHONS compounds in summer were  $22 \pm 3\%$ ,  $36 \pm 5\%$ ,  $22 \pm 3\%$ , and  $20 \pm 4\%$ , respectively. The average proportions of the four subgroups in winter were  $17 \pm 2\%$ ,  $32 \pm 4\%$ ,  $24 \pm 3\%$ , and  $27 \pm 4\%$ , re-

spectively. The CHON groups were the major components of molecular formulas; furthermore, the relative intensity of the CHON groups increased significantly in winter (Figs. S2 and S3). Studies have suggested that HULIS emitted from biomass burning can produce a high abundance of CHON compounds, and S-containing compounds were the dominant component for primary HULIS emitted from coal combustion (Zhang et al., 2021; Song et al., 2018). The higher intensity of CHON compounds in winter in this study further indicated the BB contribution. The contributions of S-containing compounds (CHOS and CHONS groups) increased in winter, which might be related to the polluted air masses transported from the northern cities with increasing coal combustion emissions in winter (Song et al., 2018). Notably, the relatively higher proportions of CHO and

CHON groups in summer were most probably related to the increasing biogenic emissions in summer, resulting in the formation of some high molecular weight oligomers or highly oxidized organonitrates, which was discussed in detail in Sect. 3.4.1 and 3.4.2 in this study.

Tables S1 and S2 in the Supplement display the composition characteristics of atmospheric HULIS in the summer and winter samples, including the relative-intensity-weighted average values of the number, molecular weight ( $MW_w$ ), elemental ratios ( $O/C_w$  and  $H/C_w$ ), double-bond equivalent ( $DBE_w$ ), aromaticity index ( $AI_w$ ), and  $DBE/C_w$ . A total of 14 387 and 15 731 peaks were detected in the summer and winter samples, respectively. The  $O/C$  and  $H/C$  ratios are commonly calculated to evaluate the oxidation degree and saturation degree of the compounds, respectively (Ning et al., 2022). The  $O/C_w$  values were in a range of 0.61–0.80, with an average value of  $0.71 \pm 0.07$  for summer samples, and in a range of 0.59–0.67, with an average value of  $0.62 \pm 0.03$  for winter samples, respectively. The higher oxidation degree of summer samples compared to winter samples indicated stronger secondary HULIS formation in summer. The  $H/C_w$  values were in a range of 1.38–1.46, with an average value of  $1.42 \pm 0.03$  for summer samples, and in a range of 1.33–1.41, with an average value of  $1.36 \pm 0.04$  for winter samples, respectively. The  $O/C_w$  and  $H/C_w$  of each molecular subgroup followed a changing trend of  $CHO < CHON < CHOS < CHONS$  compounds. Most of the S-containing compounds had a  $O/C$  value  $\geq 0.7$ , suggesting that there were large amounts of highly oxidized OSs in S-containing compounds which contained various functional groups and were mainly from the photochemical oxidation of biogenic or anthropogenic volatile organic compounds (VOCs; Mutzel et al., 2015). The double-bond equivalent (DBE) values were calculated to describe the degree of the unsaturation of compounds and restricted the assigned molecular formulas with an unreasonably high or low number of rings or double bonds (Kroll et al., 2011). The related parameter  $DBE/C$  was the double-bond equivalent of a unit of carbon, which can reflect the condensed ring structures in the compounds (Jiang et al., 2021). The higher  $DBE_w$  and  $DBE/C_w$  values of CHO and CHON compounds were found in this study, indicating the higher unsaturation degree of these two groups.

Considering that double bonds can be formed by heteroatoms, especially O atoms, whereas they make no contributions to the aromaticity of the compounds,  $AI_w$  was calculated to supplement the DBE results (Song et al., 2018; Ning et al., 2019).  $AI_w$  can eliminate the contribution of O, N, and S atoms to the  $C=C$  double-bond density of molecules. The  $AI_w$  values of different compound groups in HULIS presented the following changing trends:  $AI_w$  (CHONS)  $>$   $AI_w$  (CHON)  $>$   $AI_w$  (CHO)  $>$   $AI_w$  (CHOS) in summer and  $AI_w$  (CHON)  $>$   $AI_w$  (CHO)  $>$   $AI_w$  (CHONS)  $>$   $AI_w$  (CHOS) in winter, respectively. The formulas can be classified into three parts, based on AI values proposed by previous studies,

namely aliphatic ( $AI=0$ ), olefinic ( $0 < AI \leq 0.5$ ), and aromatic ( $AI > 0.5$ ; Koch and Dittmar, 2006; Jiang et al., 2020; Ning et al., 2019). As shown in Figs. S4 and S5, the aliphatic parts were the main components of S-containing compounds in this study, and the olefinic and aromatic parts were the main components of CHO and CHON compounds. Furthermore, the aromatic proportion of the CHO and CHON compounds significantly increased in winter, suggesting the increasing anthropogenic emissions in winter.

### 3.3 Comparative analysis using Van Krevelen diagrams

In this study, the Van Krevelen diagrams (Fig. 3) were constructed to display the molecular composition and categorical distribution of the collected samples (Noziere et al., 2015; Patriarca et al., 2018; Li et al., 2022). According to the elemental ratios ( $O/C$  and  $H/C$  ratios) and AI values, seven major compound classes were classified, including lipid-like species, lignin-like species, protein-like species, tannin-like species, carbohydrate-like species, a condensed aromatic structure, and unsaturated hydrocarbon (Table S3). The Van Krevelen diagrams showed similar distributions across the 12 samples. The CHO and CHON compounds located in the bottom-left area and the S-containing compounds located in the upper-right area have higher  $O/C$  and  $H/C$  ratios, indicating a higher degree of oxidation and saturation. The condensed aromatic structure mainly appeared in the CHO and CHON compounds, further suggesting the influence of anthropogenic emissions on the formation of CHO and CHON compounds.

Figure 4 presents the averaged relative contributions of the number of molecular formulas from the seven categories in summer and winter samples, respectively. Lignin-like species accounted for the highest proportion of CHO compounds, with average contributions of 58 % and 61 % in summer and winter, respectively, followed by CHON compounds with average contributions of 48 % and 57 % in summer and winter, respectively. Lignins are mainly composed of carboxyl groups, alicyclic rings, aromatic rings, and other O-containing groups. Previous studies have reported that lignin was a complex phenolic polymer which usually came from direct biological emissions or combustions of biofuel (Ning et al., 2019; Boreddy et al., 2021; Sun et al., 2021). Lignin pyrolysis products and other lignin-derived molecules have been shown to be oxidized into light-absorbing BrC chromophores under certain conditions (Fleming et al., 2020).

Tannin-like species accounted for 21 %, 27 %, 23 %, and 30 % of CHO, CHON, CHOS, and CHONS compounds, respectively, in summer, which were higher than those in winter, with contributions of 13 %, 16 %, 16 %, and 23 % of CHO, CHON, CHOS, and CHONS compounds, respectively. Tannin-like species are a series of polyphenolic compounds containing hydroxyls and carboxylic groups which have been widely reported in fog, cloud water, and aerosol samples, attributing to highly oxidized organic compounds,

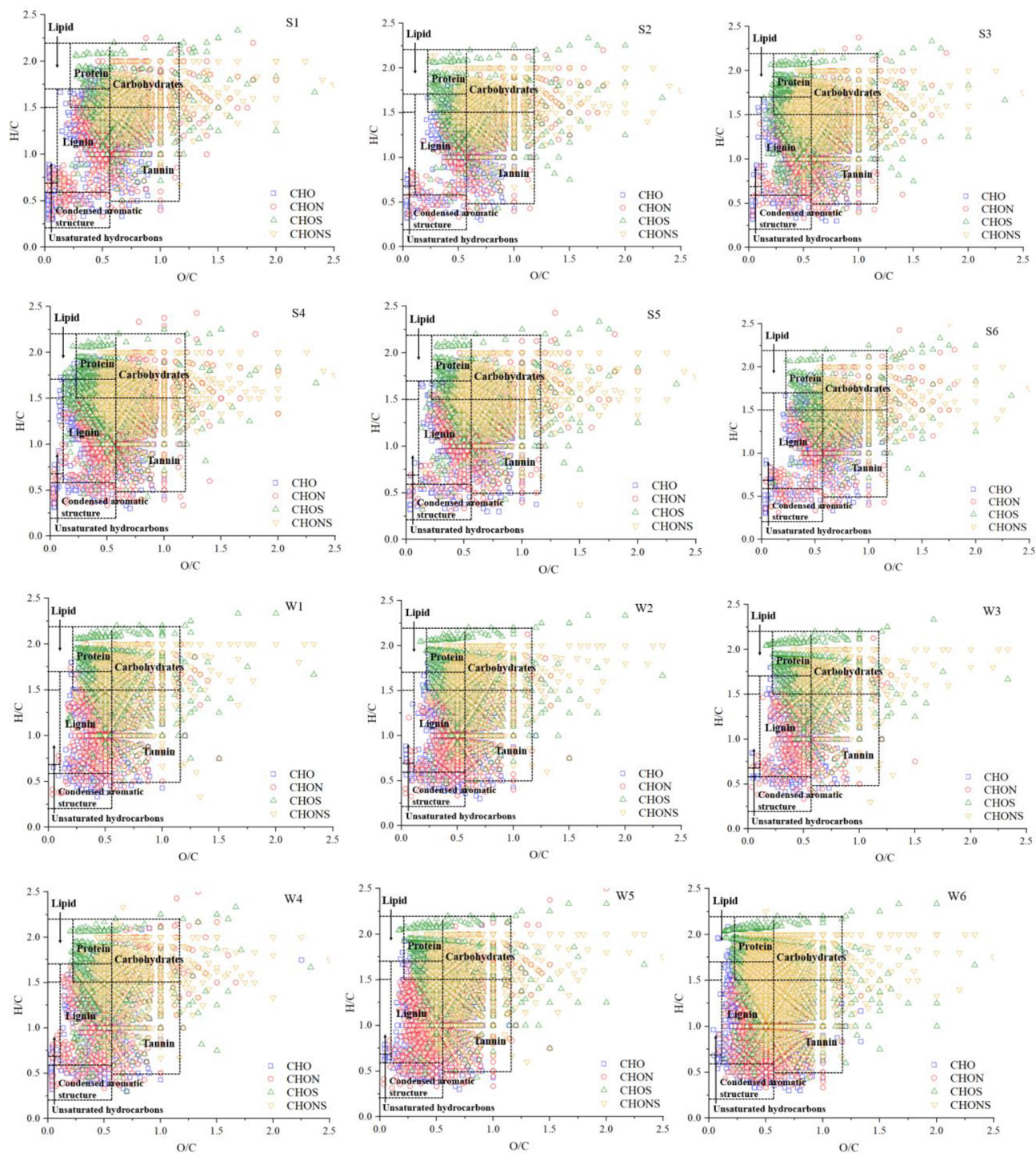


**Figure 3.** Van Krevelen diagrams of the 12 samples.

such as OSs or nitroxy-OSs, produced from the nighttime chemistry between the biogenic VOCs with  $\text{NO}_3$  (Altieri et al., 2009, 2008; Bianco et al., 2018; Ning et al., 2019; Shen et al., 2021). Carbohydrate-like species which contain monosaccharides, alditols, and anhydrosugars mainly consisted of CHONS compounds, which also had a relatively

higher proportion of 33% in summer than that of 29% in winter (Sun et al., 2021).  $\text{C}_{10}\text{H}_{16}\text{NO}_7\text{-}_9\text{S}$ , as monoterpene nitroxy-OSs, showing high relative intensities, were typical carbohydrate-like species detected in this study which represented biogenic secondary organic aerosols (SOAs; Ning et al., 2019; Surratt et al., 2008; Wang et al., 2020). Both



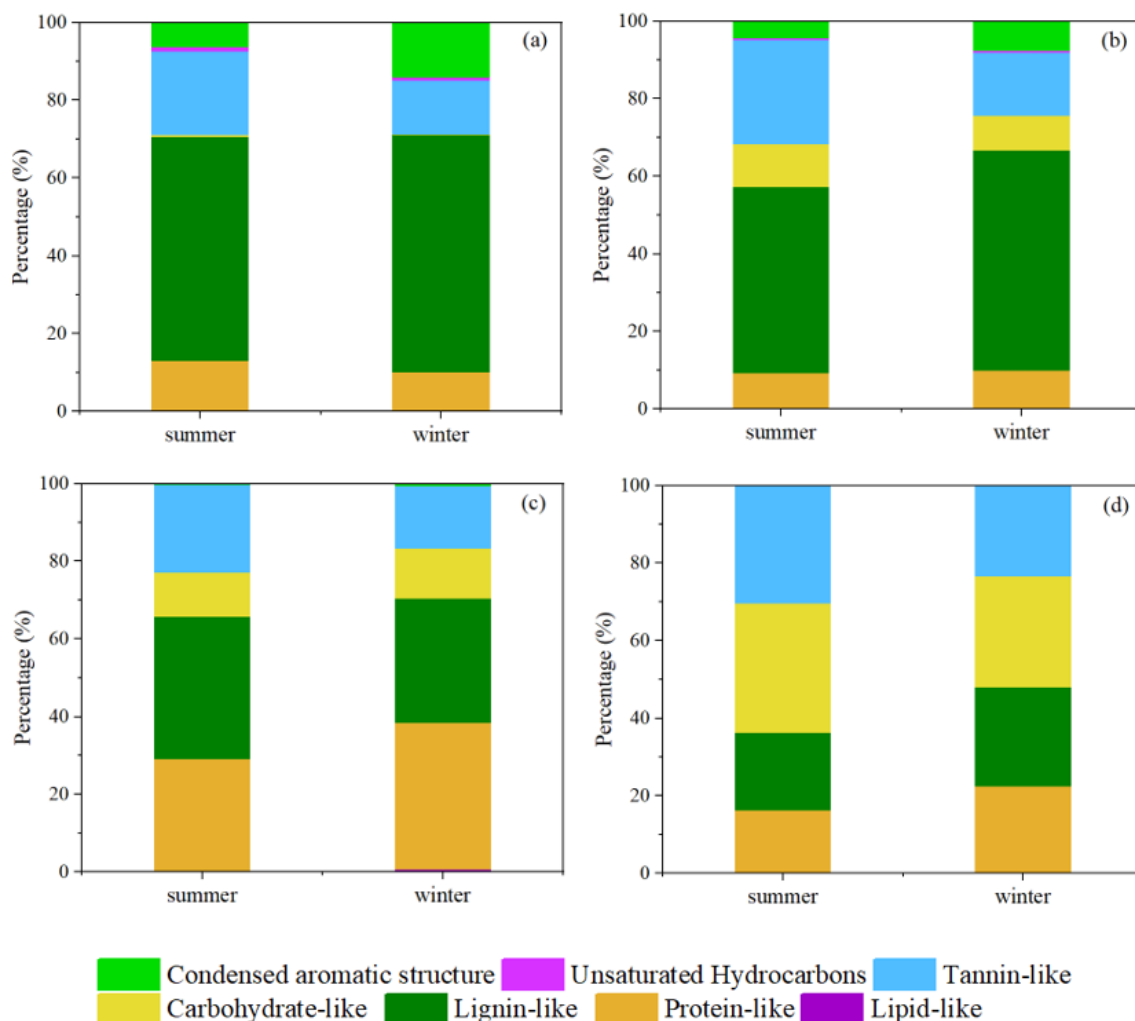


**Figure 4.** Contributions of seven categories in CHO (a), CHON (b), CHOS (c), and CHONS (d) compounds.

the higher proportions of tannin-like and carbohydrate-like classes in summer indicated stronger biogenic SOA formation in this study.

Protein-like classes mainly consisted of CHOS compounds, with average proportions of 29% and 38% in summer and winter, respectively. Proteins contain peptide-like structures formed by dehydration with different kinds of amino acids and consist of short chains of amino acid residues (Bianco et al., 2018). These compounds are associated with photochemical oxidation processing in aerosols, thus resulting in the significant formation of OSs from biogenic or anthropogenic precursors in this study (Bigg and Leck, 2008).

Higher condensed aromatics were detected in winter, with average proportions of 14% in CHO compounds and 8% in CHON compounds, respectively, which were 2–2.5 times that of those in summer. Condensed aromatics are important components of PAHs, which were usually emitted from the incomplete combustion of fossil fuels (Ma et al., 2020). The

increase in the proportion of condensed aromatics in winter indicated the stronger influence of anthropogenic sources on HULIS formation. The unsaturated hydrocarbon and lipid-like species showed the lowest molecular number percentage of less than 1% in this study. Previous studies have shown that the lipid-like species were the main components of water-insoluble organic compounds in aerosols and could be attributed to monocarboxylic acids (Ning et al., 2022; Wozniak et al., 2008).

In summary, both the summer and winter samples were mainly composed of compounds from biogenic origins (lignin-like, tannin-like, protein-like, and carbohydrate-like species). More tannin-like and carbohydrate-like species were detected in summer, including large amounts of highly oxidized OSs or nitrooxy-OSs, indicating biogenic SOA formation. More condensed aromatic structures in CHO and CHON compounds were detected in winter, owing to increasing anthropogenic emissions. It is noted that the ESI ionization technology is more sensitive to the identification



of polar compounds (Jiang et al., 2014; Lin et al., 2018). Therefore, the low polar or nonpolar compounds, such as PAHs or their derivatives from fossil fuel sources, were probably underestimated in this study.

### 3.4 Molecular composition of HULIS

#### 3.4.1 Molecular characteristics of CHO compounds

The  $O/C_w$  and  $H/C_w$  ratios for the CHO compounds were 0.45–0.56 and 1.15–1.30 for the summer samples and 0.42–0.48 and 0.90–1.02 for the winter samples (Tables S1 and S2). The summer samples showed a higher oxidation degree and saturation degree. We first plotted the Van Krevelen diagrams of the four molecular subgroups showing the relative intensities for all 12 samples, and similar distributions of the high-intensity compounds were found in the six summer samples and the six winter samples, respectively. Then we combined all of the data in summer and winter, respectively. As shown in Fig. 5a and d, the CHO compounds in summer with high relative abundance were located at the area within  $0.2 \leq O/C \leq 1.0$  and  $1.0 \leq H/C \leq 1.7$ , mainly including lignin-like species and tannin-like species, which were closely related to biogenic emissions. On the contrary, the condensed aromatics showed high relative abundance in winter, suggesting obviously different sources of HULIS in summer and winter. The DBE values increased with the increase in the C numbers (Fig. 5b and e). The high-intensity CHO compounds in HULIS had DBE values between 3–7, with C numbers from 10 to 20 for summer samples. In winter, the high-intensity CHO compounds had DBE values between 7–11, with C numbers from 5 to 15. As mentioned above, the aromatic ( $AI > 0.5$ ) proportion of the CHO compounds significantly increased in winter, and the higher DBE values in winter further indicated the presence of more highly unsaturated aromatic compounds, which reflected the anthropogenic emissions.

The CHO compounds were classified according to the number of oxygen atoms to evaluate the oxygen content. As shown in Fig. 5c and f, the high-intensity CHO compounds with 6–11 oxygen atoms were detected in summer, such as  $C_{15}H_{24}O_6$ ,  $C_{15}H_{22}O_{10}$ ,  $C_{18}H_{26}O_8$ , and  $C_{18}H_{26}O_9$ , and these highly oxygenated organic molecules with a high molecular weight have also been detected in laboratory  $\alpha$ -pinene ozonolysis SOAs (Pospisilova et al., 2020). We further classified the CHO compounds by different carbon atom numbers. As shown in Fig. S6, the  $C_{17}$ – $C_{22}$  compounds were the main components of the CHO compounds, accounting for more than 50 % of the total number of CHO molecular formulas in both summer and winter seasons. However, the total relative intensities of the CHO compounds in summer were significantly higher than those in winter, of which the  $C_{23}$ – $C_{26}$  and  $C_{27}$ – $C_{32}$  compounds were enriched in summer. These high molecular weight compounds were probably oligomers formed from various biogenic precursors, such as isoprene,

sesquiterpene, and monoterpene (Daellenbach et al., 2019; Berndt et al., 2018). The high intensities of these compounds in summer further indicated the stronger biogenic SOA formation in summer compared with that in winter.

High-intensity CHO compounds with four–nine oxygen atoms were detected in winter (Fig. 5c), of which the  $C_{14}H_{10}O_4$  formula with a DBE value of 10 appeared to have the highest intensity, which was probably functional PAHs, and have been reported in HULIS from coal combustion smoke particles (Song et al., 2019). As shown in Figs. S2 and S3, the  $C_{14}H_{10}O_4$  formula appeared to have a high intensity in all the winter samples, providing evidence of coal combustion emissions in winter. Some other high-intensity compounds in winter, such as  $C_{14}H_8O_4$  and  $C_{14}H_8O_5$ , both with DBE values of 11, and  $C_{13}H_8O_2$ ,  $C_{13}H_8O_5$ , and  $C_{13}H_8O_6$ , with DBE values of 10, might refer to hydroxyl substitutions derived from anthracenedione and xanthone, respectively, which have been reported in secondary wood combustion products (Bruns et al., 2015).  $C_{15}H_{10}O_6$ ,  $C_{15}H_8O_6$ , and  $C_{16}H_{12}O_7$ , which had DBE values of 11, 12, and 11, respectively, might be flavonoids which had a flavone backbone, the key structure of plant pigments that exists widely in plants in nature, and could be important sources of BrC chromophores in aged BBOAs (Fleming et al., 2020; Lin et al., 2016; Huang et al., 2021). Phenolic substances derived from phenol, guaiacol, and syringol also exist widely in BBOAs, usually from the pyrolysis of lignins in wood, which also play an important role in aqueous-phase SOA formation (Boreddy et al., 2021). For instance,  $C_{13}H_{10}O_3$  and  $C_{13}H_{10}O_5$  are guaiacol derivatives,  $C_{15}H_{16}O_8$  are syringol derivatives, and  $C_{18}H_{14}O_6$  and  $C_{18}H_{14}O_7$  are phenol derivatives (Sun et al., 2021). As shown in Fig. S7, the relative intensities of the CHO compounds mentioned above that are produced from BB were found to have similar trends with the mass concentrations of levoglucosan, which were significantly higher in W1–W3 samples, corresponding to the BB period from 31 December 2017 to 1 January 2018, providing evidence of the BB influence on HULIS formation in winter.

It is noted that the top compounds of  $C_9H_6O_7$  and  $C_{10}H_6O_8$  were detected both in the summer and winter samples (Figs. S2 and S3), which had DBE values of 7 and 8, respectively, containing abundant condensed aromatic ring structures with high O numbers. Their peaks were also detected in the HFO (heavy fuel oil)-fueled off-road engine samples reported before, suggesting that the traffic emissions contribute to HULIS (Cui et al., 2019). This supported the radiocarbon analysis results in this study and gave further information showing that the traffic emissions were important fossil fuel sources in both summer and winter seasons, which was also found in previous research that reported on the sources of HULIS based on the positive matrix factorization (PMF) model by Bao et al. (2022).

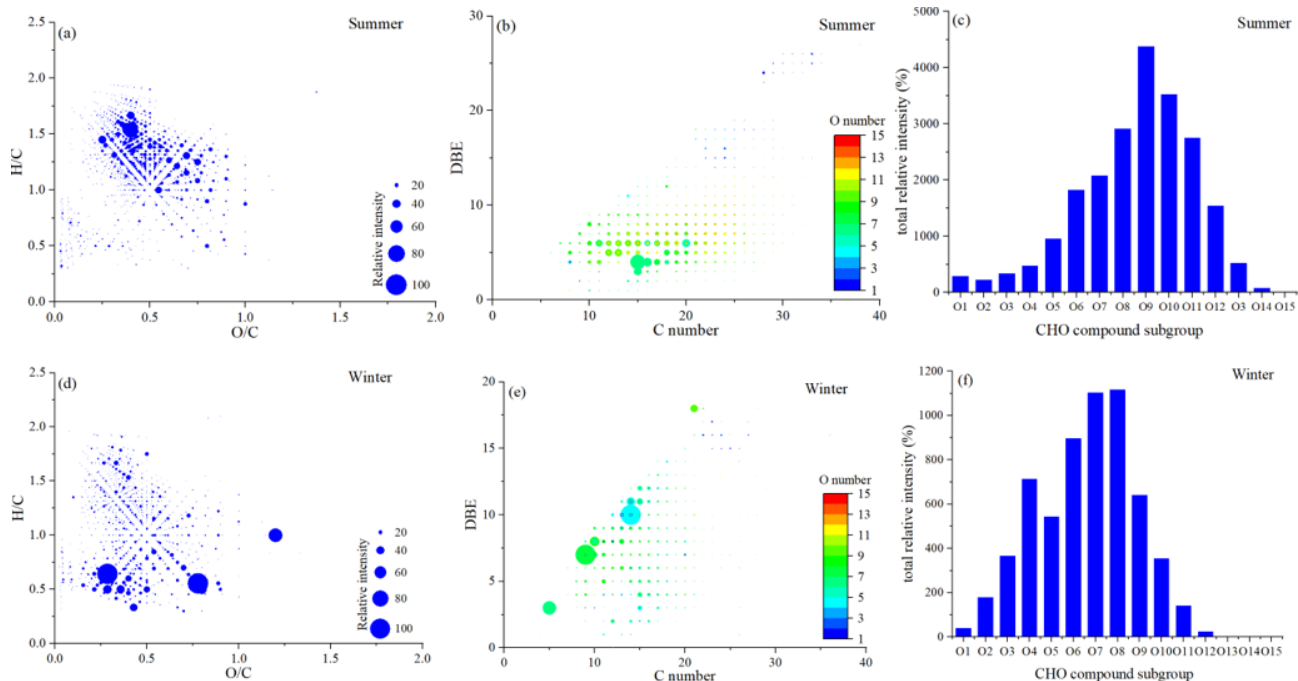


**Figure 5.** Van Krevelen diagram (a,d), plot of DBE values vs. carbon atom numbers (b,e), and the total relative intensity of each subgroup (c,f) for the CHO compounds in summer and winter.

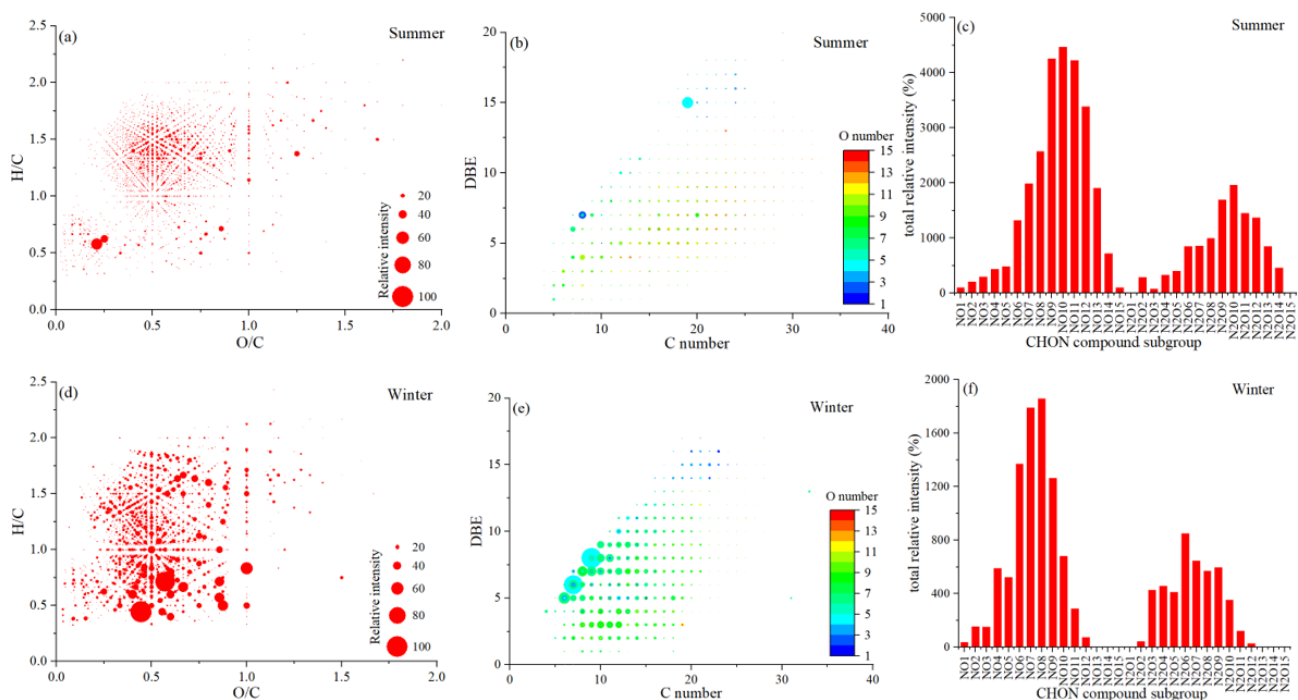


**Figure 6.** Van Krevelen diagram (a,d), plot of DBE values vs. carbon atom numbers (b,e), and the total relative intensity of each subgroup (c,f) for the CHON compounds in summer and winter.

### 3.4.2 Molecular characteristics of CHON compounds

The  $O/C_w$  of CHON compounds in summer and winter were 0.57–0.71 and 0.52–0.56, respectively, while the  $H/C_w$  were 1.20–1.32 and 1.00–1.11, respectively (Tables S1 and S2). Compared with the summer CHON compounds, the winter CHON compounds presented a significantly higher ion abundance (Fig. 6a and d). The most abundant CHON subgroups had DBE values of 4–7 and 3–10 in summer and winter, respectively (Fig. 6b and e). Similar to the CHO compounds, the higher DBE values of high-intensity CHON compounds in HULIS in winter indicated a high prevalence of double bonds or ring structures. According to the N and O number, the CHON compounds were classified into  $N_1O_x$  ( $N_1O_1$ – $N_1O_{15}$ ) and  $N_2O_x$  ( $N_2O_2$ – $N_2O_{14}$ ) subgroups in summer and  $N_1O_x$  ( $N_1O_1$ – $N_1O_{12}$ ) and  $N_2O_x$  ( $N_2O_2$ – $N_2O_{12}$ ) subgroups in winter, respectively (Fig. 6c and f).  $NO_{8-12}$  and  $NO_{6-9}$  compounds were mostly enriched subgroups in summer and winter, respectively. More oxygen-enriched CHON compounds containing an O number above nine were detected in summer, implying a higher oxidation degree for summer samples. In addition, the  $N_1O_x$  values were both major compounds and represented an average of  $64 \pm 4\%$  and  $61 \pm 6\%$  of the CHON molecular formulas in summer and winter, respectively, indicating the presence of more single nitro/amino substituents in CHON compounds in this study.

Among the CHON compounds,  $95 \pm 1\%$  and  $86 \pm 3\%$  of the CHON compounds had O/N values  $\geq 3$  in summer and winter, respectively, in this study, indicating that these compounds contained large amounts of oxidized nitrogen functional groups such as nitro compounds ( $-NO_2$ ) and/or organonitrates ( $-ONO_2$ ), and excess oxygen atoms indicated the existence of other oxygen-containing functional groups (Laskin et al., 2009). The organonitrate formation from the  $NO_3$  oxidation of biogenic or anthropogenic VOCs can affect the interactions between anthropogenic and natural emissions (He et al., 2021; Shen et al., 2021; Wang et al., 2020). Organonitrates were found to be important species contributing to SOA formation in the polluted urban environment, which were enhanced under high  $NO_x$  levels (Zheng et al., 2021). The significantly higher relative intensities of CHON compounds in winter indicated that the high  $NO_x$  environment in winter promoted the formation of organonitrates and highlighted the importance of organonitrates for SOA control in a polluted environment.

Furthermore, we found that the increase in the relative abundance of CHON compounds in winter was particularly significant in the W1–W3 samples (Figs. S2 and S3) corresponding to the BB episode. Phenols produced from the pyrolysis of lignins can react with  $NO_3$  radicals in the atmosphere, producing nitrophenols, which have been shown to be important BrC chromophores in BBOAs (Y. Wang et al., 2017; Lin et al., 2016; Cai et al., 2020). It was reported that the gas-phase reactions of  $NO_3$  radicals with phenolic substances occurred at least 4 orders of magni-

tude faster than those with aromatic hydrocarbon and even faster in the aqueous phase (Lin et al., 2017). Among the top CHON compounds with high relative abundance in W1–W3 samples, such as  $C_6H_4N_2O_6$  and  $C_7H_6N_2O_6$ , both with a DBE value of 6, there were references to nitrophenols containing one or two nitrogen-containing functional groups, which have been widely reported in aged BBOAs, indicating that the increase in the CHON compounds' relative intensity in the W1–W3 samples was closely related to BB (Lin et al., 2017, 2016; Cai et al., 2020; Mohr et al., 2013; Kourtchev et al., 2016). Some other top CHON compounds in winter samples, such as  $C_9H_4NO_4$  and  $C_{10}H_6NO_4$  with low O/C and H/C ratios, most likely indicated the presence of condensed aromatic structures in the compounds. The  $C_9H_4NO_4$  compounds were most likely emitted from vehicle emissions, which have previously been reported (Cui et al., 2019).

It is worth noting that some high-intensity CHON compounds with low O/C and H/C ratios were detected in summer samples in this study (Fig. 6a), which were closely related to aromatic compounds from anthropogenic emissions. The top compounds with molecular formulas of  $C_8H_5N_2O_2$  and  $C_{19}H_{11}N_2O_4$ , which had O/N of 1 and 2, respectively, were both reduced N compounds referring to N-heterocyclic compounds. Previously, studies have found that the N-heterocyclic aromatic compounds can be formed through the aldehyde–ammonia reactions (De Haan et al., 2018; R. Zhang et al., 2022). This indicated the important role of reduced N species (e.g., ammonium) in the formation of anthropogenic SOA in summer. Our results were consistent with a previous study conducted in Xi'an, China, which also found that the formation of reduced N compounds in light-absorbing aerosols through ammonia involved reactions in summer (Zeng et al., 2021).

### 3.4.3 Molecular characteristics of S-containing compounds (CHOS and CHONS compounds)

The  $O/C_w$  of CHOS compounds in summer and winter were 0.60–0.79 and 0.56–0.67, respectively, while the  $H/C_w$  were 1.50–1.54 and 1.53–1.72, respectively. The  $O/C_w$  of CHONS compounds in summer and winter were 0.82–1.01 and 0.76–0.94, respectively, while the  $H/C_w$  were 1.57–1.65 and 1.58–1.66, respectively (Tables S1 and S2). As shown in Figs. 7a and d and 8a and d, the high-intensity S-containing compounds in summer and winter were both located at the area where  $O/C > 0.5$  and  $H/C > 1.5$ , respectively. In addition, the relative intensity of S-containing compounds increased with the O/C ratios, suggesting that the S-containing compounds were highly oxidized. A small number of high-intensity S-containing compounds with  $O/C < 1.0$  and  $H/C < 1.0$  were also found in winter in this study, which might be related to OSs and nitrooxy-OSs produced from the oxidation of aromatic hydrocarbon. The CHOS compounds presenting a high relative abundance were rich in  $O_{6-9}S$  and  $O_{5-7}S$  groups in summer and winter, respectively, of which

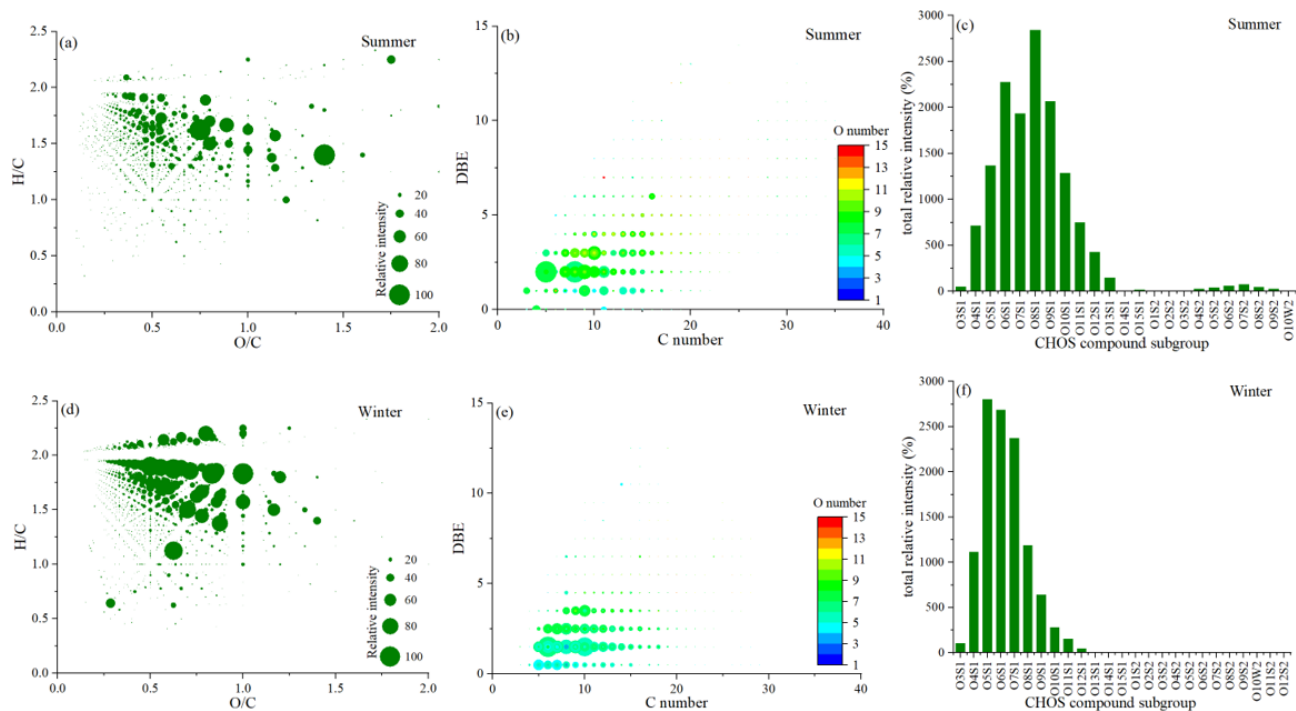


**Figure 7.** Van Krevelen diagram (a, d), plot of DBE values vs. carbon atom numbers (b, e), and the total relative intensity of each subgroup (c, f) for the CHOS compounds in summer and winter.

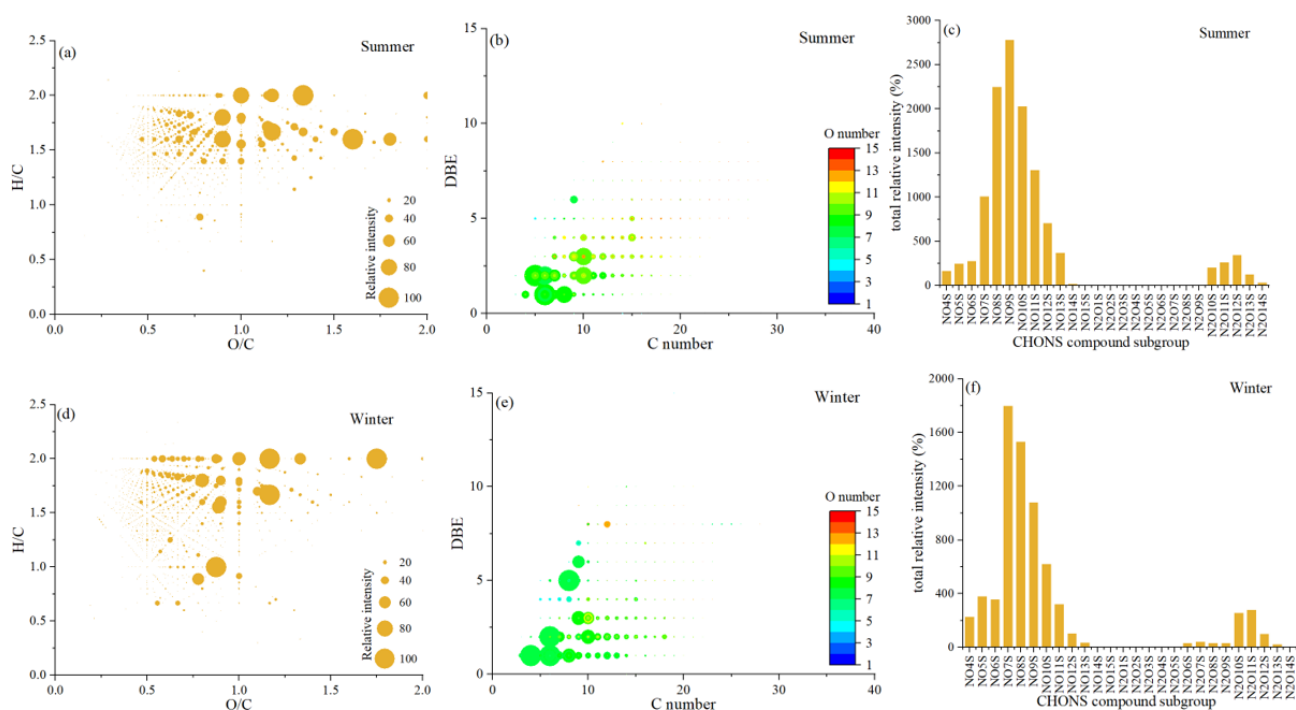


**Figure 8.** Van Krevelen diagram (a, d), plot of DBE values vs. carbon atom numbers (b, e), and the total relative intensity of each subgroup (c, f) for the CHONS compounds in summer and winter.



the DBE values were all below 4. The CHONS compounds were rich in  $O_{8-10}S$  and  $O_{7-9}S$  groups in summer and winter, respectively, of which the DBE values were all below 6 (Fig. 7b, e, c, f and 8b, e, c, f). Compared with those of the CHO and CHON compounds, the DBE values of S-containing compounds were significantly lower.

Among the S-containing compounds, more than 95 % of the CHOS,  $CHON_1S$ , and  $CHON_2S$  formulas had O/S ratios greater than 4, 7, and 10, respectively, implying that these compounds may contain organic sulfate functional groups ( $-OSO_3$ ) or one or two organic nitrate groups ( $-ONO_2$ ) and that these compounds were more likely OSs or nitrooxy-OSs, presenting lower DBE values and higher O/C and H/C ratios (Tables S4 and S5; O'Brien et al., 2014). The high-intensity CHONS compounds observed in this study, such as  $C_{10}H_{16}NO_{7-9}S$ ,  $C_{10}H_{18}NO_{8-9}S$ ,  $C_{10}H_{18}N_2O_{11}S$ , and  $C_9H_{14}NO_{8-9}S$  could be nitrooxy-OSs derived from monoterpenes such as limonene and  $\alpha$ -terpinene, for which we found that the formulas in summer contained more oxygen atoms, indicating the higher oxidation degree of these nitrooxy-OSs in summer (Figs. S2 and S3; Sun et al., 2021; Bruggemann et al., 2020; Wang et al., 2020; Y. Wang et al., 2018).

The CHOS compounds with high-intensity abundance, such as typical isoprene epoxydiol (IEPOX)-derived OSs with molecular formulas of  $C_5H_8O_7S$  and  $C_5H_{10}O_7S$ , were both detected in the summer and winter samples, of which the relative intensity of  $C_5H_8O_7S$  was over 80 % in the S1, S2, S5, and S6 samples, indicating the significant isoprene SOA formation in summer (Kourtchev et al., 2016, 2013). The results were consistent with the PMF results reported by Bao et al. (2022). The monoterpene-derived OSs, such as  $C_8H_{14}O_6S$ ,  $C_8H_{14}O_8S$ ,  $C_{10}H_{18}O_8$ ,  $C_{10}H_{14}O_6$ , and  $C_{11}H_{16}O_7$ , were detected in both summer and winter samples in this study, which could refer to monoterpene-OSs derived from  $\alpha$ -pinene,  $\alpha$ -terpinene, and limonene (Wang et al., 2020). Moreover, OSs with high carbon numbers ( $C \geq 14$ ), such as  $C_{14}H_{22}O_7S$ ,  $C_{14}H_{22}O_8S$ ,  $C_{14}H_{24}O_7S$ ,  $C_{15}H_{26}O_7S$ ,  $C_{15}H_{24}O_7S$ ,  $C_{15}H_{24}O_8S$ , and  $C_{16}H_{28}O_7S$ , were also observed in both the summer and winter samples. Long-chain alkanes emitted from vehicle emissions might be precursors of these OSs, which was consistent with the molecular structures of the OSs collected in urban areas affected by traffic emissions such as Shanghai, Los Angeles, and Beijing (K. Wang et al., 2019; Tao et al., 2014; X. K. Wang et al., 2016). The aromatic OSs such as naphthalene-derived OSs with molecular formulas of  $C_{10}H_{10}O_6S$ ,  $C_{10}H_{10}O_7S$ , and  $C_{10}H_{12}O_7S$ , 2-methylnaphthalene-derived OSs with molecular formulas of  $C_9H_{12}O_6S$ ,  $C_{11}H_{12}O_7S$ , and  $C_{11}H_{14}O_7S$ , and hydroxybenzene-derived OSs with molecular formulas of  $C_6H_6O_5S$  were also observed in this study (Qi et al., 2021; Riva et al., 2015; Blair et al., 2017). Figure S8 further displays the ternary plot of the relative intensities of OSs from biogenic precursors (e.g., isoprene and monoterpenes), long-chain alkanes, and aromatic hydrocarbon. As

shown in Fig. S8, the biogenic OS and long-chain alkane OS formation were comparable in summer and winter, demonstrating the biogenic and anthropogenic emission contributions to HULIS. The aromatic OSs presented higher relative intensities in winter, further indicating the increasing anthropogenic emissions in winter. The presence of long-chain alkane-derived OSs in both summer and winter seasons provided more evidence that traffic emissions were one of the important fossil fuel sources of HULIS in this study.

### 3.5 Comparison with organic compounds in source and atmospheric aerosol samples

The O/C and H/C ratios of water-soluble HULIS in this study were compared with those of water-soluble organic compounds reported in source samples from BB, coal combustion, vehicle emissions (Tang et al., 2020; Song et al., 2018, 2019; Cui et al., 2019), cloud water samples (Bianco et al., 2018; Zhao et al., 2013), rainwater samples (Altieri et al., 2009), and fog samples (Brege et al., 2018; Fig. 9). In addition, the O/C and H/C ratios of organic fraction in aerosol samples collected in Beijing (Jang et al., 2020; C. Wu et al., 2019; J. Wang et al., 2018), Tianjin (Han et al., 2022), Baoding (Sun et al., 2021), Shanghai (X. Wang et al., 2017), and Guangzhou (Jiang et al., 2021), respectively, in China, Mainz, (K. Wang et al., 2018), Cork city (Kourtchev et al., 2014), and Bologna (Brege et al., 2018), respectively, in Europe, and Bakersfield (O'Brien et al., 2014) and Virginia (Willoughby et al., 2014), respectively, in the USA were also shown in Fig. 9. The O/C ratios were obviously higher than those detected in the primary BB, coal combustion, and vehicle emission samples. The H/C ratios of the CHO and CHON compounds were comparable with the source samples, indicating that the organics in HULIS experienced secondary atmospheric processes and the mixed sources of HULIS in this study. The H/C ratios of the S-containing compounds were much higher than those of source samples, which could be attributed to the significant organosulfates formation in the atmosphere.

The O/C ratios reported in this study were also higher than those reported in aerosol samples in urban area in China, further indicating the serious secondary pollution in Nanjing, China. Among the CHO and CHON compounds, we found that the highest H/C ratio values were observed in the southern city of Guangzhou, followed by those in Nanjing and Shanghai, and the lowest values were observed in northern cities such as Beijing, Tianjin, and Baoding, indicating the higher unsaturation degree of the aerosol samples collected from the northern cities, which were also considered to be in the heavy industrial region in China. The higher H/C ratios of aerosol samples collected in Europe and the USA indicated fewer anthropogenic emissions such as industrial emissions from those areas.

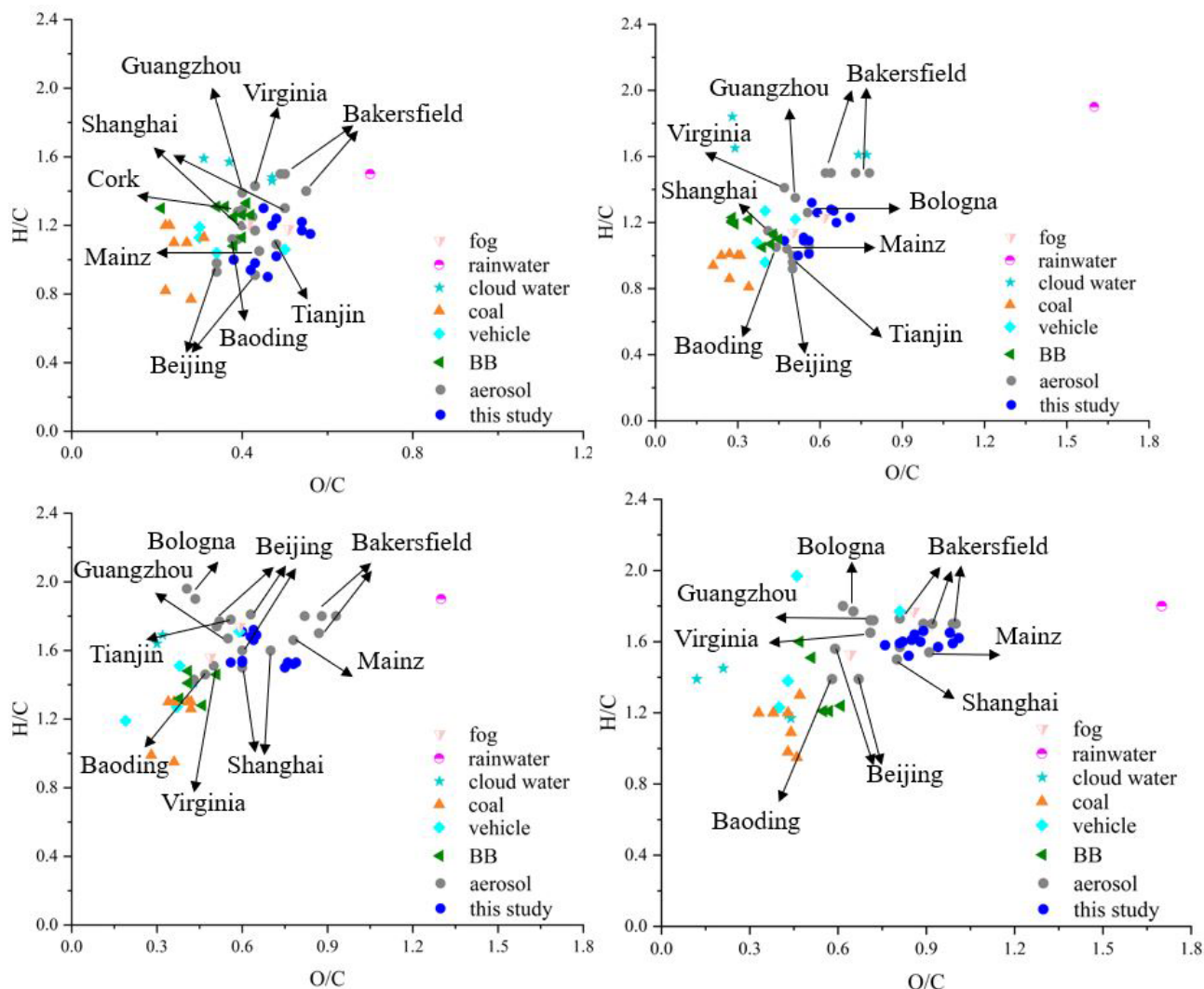


**Figure 9.** Comparison of O/C and H/C ratios of water-soluble organic compounds in different atmospheric media in CHO (a), CHON (b), CHOS (c), and CHONS (d) compounds.

#### 4 Conclusions

This study focuses on the sources and molecular characteristic differences in the water-soluble HULIS in summertime and wintertime from 2017 to 2018 at a suburban site in the YRD, China, based on radiocarbon analysis and FT-ICR-MS measurements with an ESI ion source in the negative mode. The carbon isotope analysis results highlight the important fossil fuel source contributions to HULIS at the study site. A total of 14 387 and 15 731 peaks were detected in the summer and winter samples, respectively, based on the FT-ICR-MS results. The assigned molecular formulas were classified into CHO, CHON, CHOS, and CHONS subgroups, according to their elemental compositions. The Van Krevelen diagrams showed that more tannin-like and carbohydrate-like species were detected in summer, indicating biogenic SOA formation, whereas more compounds containing con-

densed aromatic structures were detected in winter, which were derived from anthropogenic emissions. The total relative intensity of CHO compounds in summer was significantly higher than those in winter, which contain lots of macromolecular oligomers derived from biogenic precursors. The high-intensity CHO compounds in winter were mainly aromatic compounds such as phenolic substances and flavonoids, which were related to aged BBOAs and oxidized PAHs that were most probably from fossil fuel combustion. On the contrary, the total relative intensity of CHON compounds significantly increased in winter and were mainly composed of nitro compounds or organonitrates. The enhanced formation of nitrophenols in winter indicated the BB influence. The increasing organonitrate formation in winter highlighted the secondary N-containing compound formation via  $\text{NO}_3$  radical-initiated oxidation pro-

cesses. It is worth noting that the top CHON compounds in summer were referring to aromatic-reduced N compounds produced from the aldehyde–ammonia reactions. The S-containing compounds were mainly composed of highly oxidized OSs. The monoterpene-derived OSs and long-chain alkane-derived OSs were widely observed in both summer and winter samples, while the aromatic OS formation was found to be more significant in winter. The presence of long-chain alkane-derived OSs supported the radiocarbon results, indicating that the traffic emissions were important fossil fuel sources at the study site. The presence of aromatic secondary N-containing and S-containing compounds provided evidence for the substantial contributions from anthropogenic SOA formation to fossil fuel sources at the study site. These results further verified the work reported before by Bao et al. (2022), based on the PMF model, which found significant anthropogenic SOA and fossil fuel combustion contributions to HULIS in urban areas in China at the molecular level. In addition, strong biogenic emission in summer and BB in winter were found in this study, highlighting the importance of different control policies for each season in the future.

**Code and data availability.** Code and data are available upon request to the corresponding author (dryanlinzhang@outlook.com).

**Supplement.** The supplement related to this article is available online at: <https://doi.org/10.5194/acp-23-8305-2023-supplement>.

**Author contributions.** YLZ designed the research. MB and FC collected the samples. MB, FC, YH and XY performed the chemical analysis. HJ and ZC performed the radiocarbon and FT-ICR-MS analysis. MB wrote the paper under the guidance of YLZ, FC, YCL, MY and RX. All authors were actively involved in the discussion of the paper.

**Competing interests.** The contact author has declared that none of the authors has any competing interests.

**Disclaimer.** Publisher's note: Copernicus Publications remains neutral with regard to jurisdictional claims in published maps and institutional affiliations.

**Financial support.** This research has been supported by the National Natural Science Foundation of China (grant nos. 42192512, 41977305, and 42273087).

**Review statement.** This paper was edited by Kimitaka Kawamura and reviewed by three anonymous referees.

## References

- Aiona, P. K., Luek, J. L., Timko, S. A., Powers, L. C., Gonsior, M., and Nizkorodov, S. A.: Effect of photolysis on absorption and fluorescence spectra of light-absorbing secondary organic aerosols, *ACS Earth Space Chem.*, 2, 235–245, <https://doi.org/10.1021/acsearthspacechem.7b00153>, 2018.
- Altieri, K. E., Seitzinger, S. P., Carlton, A. G., Turpin, B. J., Klein, G. C., and Marshall, A. G.: Oligomers formed through in-cloud methylglyoxal reactions: Chemical composition, properties, and mechanisms investigated by ultra-high resolution FT-ICR mass spectrometry, *Atmos. Environ.*, 42, 1476–1490, <https://doi.org/10.1016/j.atmosenv.2007.11.015>, 2008.
- Altieri, K. E., Turpin, B. J., and Seitzinger, S. P.: Oligomers, organosulfates, and nitrooxy organosulfates in rainwater identified by ultra-high resolution electrospray ionization FT-ICR mass spectrometry, *Atmos. Chem. Phys.*, 9, 2533–2542, <https://doi.org/10.5194/acp-9-2533-2009>, 2009.
- Bao, M., Zhang, Y. L., Cao, F., Lin, Y. C., Hong, Y., Fan, M., Zhang, Y., Yang, X., and Xie, F.: Light absorption and source apportionment of water soluble humic-like substances (HULIS) in PM<sub>2.5</sub> at Nanjing, China, *Environ. Res.*, 206, 112554, <https://doi.org/10.1016/j.envres.2021.112554>, 2022.
- Berndt, T., Mender, B., Scholz, W., Fischer, L., Herrmann, H., Kulmala, M., and Hansel, A.: Accretion product formation from ozonolysis and OH radical reaction of alpha-Pinene: mechanistic insight and the influence of isoprene and ethylene, *Environ. Sci. Technol.*, 52, 11069–11077, <https://doi.org/10.1021/acs.est.8b02210>, 2018.
- Bianco, A., Deguillaume, L., Vaitilingom, M., Nicol, E., Baray, J. L., Chaumerliac, N., and Bridoux, M.: Molecular characterization of cloud water samples collected at the Puy de Dome (France) by Fourier transform ion cyclotron resonance mass spectrometry, *Environ. Sci. Technol.*, 52, 10275–10285, <https://doi.org/10.1021/acs.est.8b01964>, 2018.
- Bigg, E. K. and Leck, C.: The composition of fragments of bubbles bursting at the ocean surface, *J. Geophys. Res.*, 113, D11209, <https://doi.org/10.1029/2007jd009078>, 2008.
- Blair, S. L., MacMillan, A. C., Drozd, G. T., Goldstein, A. H., Chu, R. K., Pasa-Tolic, L., Shaw, J. B., Tolic, N., Lin, P., Laskin, J., Laskin, A., and Nizkorodov, S. A.: Molecular characterization of organosulfur compounds in biodiesel and diesel fuel secondary organic aerosol, *Environ. Sci. Technol.*, 51, 119–127, <https://doi.org/10.1021/acs.est.6b03304>, 2017.
- Boreddy, S. K. R., Hegde, P., Aswini, A. R., and Aryasree, S.: Chemical characteristics, size distributions, molecular composition, and brown carbon in South Asian outflow to the Indian Ocean, *Earth Space Sci.*, 8, e2020EA001615, <https://doi.org/10.1029/2020ea001615>, 2021.
- Brege, M., Paglione, M., Gilardoni, S., Decesari, S., Facchini, M. C., and Mazzoleni, L. R.: Molecular insights on aging and aqueous-phase processing from ambient biomass burning emissions-influenced Po Valley fog and aerosol, *Atmos. Chem. Phys.*, 18, 13197–13214, <https://doi.org/10.5194/acp-18-13197-2018>, 2018.
- Bruggemann, M., Xu, R., Tilgner, A., Kwong, K. C., Mutzel, A., Poon, H. Y., Otto, T., Schaefer, T., Poulain, L., Chan, M. N., and Herrmann, H.: Organosulfates in ambient aerosol: state of knowledge and future research directions on formation, abun-

- dance, fate, and importance, *Environ. Sci. Technol.*, 54, 3767–3782, <https://doi.org/10.1021/acs.est.9b06751>, 2020.
- Bruns, E. A., Krapf, M., Orasche, J., Huang, Y., Zimmermann, R., Drinovec, L., Močnik, G., El-Haddad, I., Slowik, J. G., Dommen, J., Baltensperger, U., and Prévôt, A. S. H.: Characterization of primary and secondary wood combustion products generated under different burner loads, *Atmos. Chem. Phys.*, 15, 2825–2841, <https://doi.org/10.5194/acp-15-2825-2015>, 2015.
- Cai, J., Zeng, X., Zhi, G., Gligorovski, S., Sheng, G., Yu, Z., Wang, X., and Peng, P.: Molecular composition and photochemical evolution of water-soluble organic carbon (WSOC) extracted from field biomass burning aerosols using high-resolution mass spectrometry, *Atmos. Chem. Phys.*, 20, 6115–6128, <https://doi.org/10.5194/acp-20-6115-2020>, 2020.
- Cao, M., Yu, W., Chen, M., and Chen, M.: Characterization of nitrated aromatic compounds in fine particles from Nanjing, China: Optical properties, source allocation, and secondary processes, *Environ. Pollut.*, 316, 120650, <https://doi.org/10.1016/j.envpol.2022.120650>, 2023.
- Chen, Q., Ikemori, F., Higo, H., Asakawa, D., and Mochida, M.: Chemical structural characteristics of HULIS and other fractionated organic matter in urban aerosols: results from mass spectral and FT-IR analysis, *Environ. Sci. Technol.*, 50, 1721–1730, <https://doi.org/10.1021/acs.est.5b05277>, 2016.
- Chen, Y., Ge, X., Chen, H., Xie, X., Chen, Y., Wang, J., Ye, Z., Bao, M., Zhang, Y., and Chen, M.: Seasonal light absorption properties of water-soluble brown carbon in atmospheric fine particles in Nanjing, China, *Atmos. Environ.*, 187, 230–240, <https://doi.org/10.1016/j.atmosenv.2018.06.002>, 2018.
- Chung, C. E., Ramanathan, V., and Decremmer, D.: Observationally constrained estimates of carbonaceous aerosol radiative forcing, *P. Natl. Acad. Sci. USA*, 109, 11624–11629, <https://doi.org/10.1073/pnas.1203707109>, 2012.
- Cui, F., Pei, S., Chen, M., Ma, Y., and Pan, Q.: Absorption enhancement of black carbon and the contribution of brown carbon to light absorption in the summer of Nanjing, China, *Atmos. Pollut. Res.*, 12, 480–487, <https://doi.org/10.1016/j.apr.2020.12.008>, 2021.
- Cui, M., Li, C., Chen, Y., Zhang, F., Li, J., Jiang, B., Mo, Y., Li, J., Yan, C., Zheng, M., Xie, Z., Zhang, G., and Zheng, J.: Molecular characterization of polar organic aerosol constituents in off-road engine emissions using Fourier transform ion cyclotron resonance mass spectrometry (FT-ICR MS): implications for source apportionment, *Atmos. Chem. Phys.*, 19, 13945–13956, <https://doi.org/10.5194/acp-19-13945-2019>, 2019.
- Daellenbach, K. R., Kourichev, I., Vogel, A. L., Bruns, E. A., Jiang, J., Petäjä, T., Jaffredo, J.-L., Aksoyoglu, S., Kalberer, M., Baltensperger, U., El Haddad, I., and Prévôt, A. S. H.: Impact of anthropogenic and biogenic sources on the seasonal variation in the molecular composition of urban organic aerosols: a field and laboratory study using ultra-high-resolution mass spectrometry, *Atmos. Chem. Phys.*, 19, 5973–5991, <https://doi.org/10.5194/acp-19-5973-2019>, 2019.
- De Haan, D. O., Tapavicza, E., Riva, M., Cui, T., Surratt, J. D., Smith, A. C., Jordan, M. C., Nilakantan, S., Almodovar, M., Stewart, T. N., de Loera, A., De Haan, A. C., Cazaunau, M., Gratien, A., Pangui, E., and Doussin, J. F.: Nitrogen-containing, light-absorbing oligomers produced in aerosol particles exposed to methylglyoxal, photolysis, and cloud cycling, *Environ. Sci. Technol.*, 52, 4061–4071, <https://doi.org/10.1021/acs.est.7b06105>, 2018.
- Fan, X., Song, J., and Peng, P. a.: Temporal variations of the abundance and optical properties of water soluble Humic-Like Substances (HULIS) in PM<sub>2.5</sub> at Guangzhou, China, *Atmos. Res.*, 172–173, 8–15, <https://doi.org/10.1016/j.atmosres.2015.12.024>, 2016.
- Fleming, L. T., Lin, P., Roberts, J. M., Selimovic, V., Yokelson, R., Laskin, J., Laskin, A., and Nizkorodov, S. A.: Molecular composition and photochemical lifetimes of brown carbon chromophores in biomass burning organic aerosol, *Atmos. Chem. Phys.*, 20, 1105–1129, <https://doi.org/10.5194/acp-20-1105-2020>, 2020.
- Glasius, M., Thomsen, D., Wang, K., Iversen, L. S., Duan, J., and Huang, R. J.: Chemical characteristics and sources of organosulfates, organosulfonates, and carboxylic acids in aerosols in urban Xi'an, Northwest China, *Sci. Total. Environ.*, 151187, <https://doi.org/10.1016/j.scitotenv.2021.151187>, 2021.
- Graber, E. R. and Rudich, Y.: Atmospheric HULIS: How humic-like are they? A comprehensive and critical review, *Atmos. Chem. Phys.*, 6, 729–753, <https://doi.org/10.5194/acp-6-729-2006>, 2006.
- Gu, C., Cui, S., Ge, X., Wang, Z., Chen, M., Qian, Z., Liu, Z., Wang, X., and Zhang, Y.: Chemical composition, sources and optical properties of nitrated aromatic compounds in fine particulate matter during winter foggy days in Nanjing, China, *Environ. Res.*, 212, 113255, <https://doi.org/10.1016/j.envres.2022.113255>, 2022.
- Han, H., Feng, Y., Chen, J., Xie, Q., Chen, S., Sheng, M., Zhong, S., Wei, W., Su, S., and Fu, P.: Acidification impacts on the molecular composition of dissolved organic matter revealed by FT-ICR MS, *Sci. Total. Environ.*, 805, 150284, <https://doi.org/10.1016/j.scitotenv.2021.150284>, 2022.
- He, Q., Tomaz, S., Li, C., Zhu, M., Meidan, D., Riva, M., Laskin, A., Brown, S. S., George, C., Wang, X., and Rudich, Y.: Optical properties of secondary organic aerosol produced by nitrate radical oxidation of biogenic volatile organic compounds, *Environ. Sci. Technol.*, 55, 2878–2889, <https://doi.org/10.1021/acs.est.0c06838>, 2021.
- Huang, L., Liu, T., and Grassian, V. H.: Radical-initiated formation of aromatic organosulfates and sulfonates in the aqueous phase, *Environ. Sci. Technol.*, 54, 11857–11864, <https://doi.org/10.1021/acs.est.0c05644>, 2020.
- Huang, R.-J., Yang, L., Shen, J., Yuan, W., Gong, Y., Ni, H., Duan, J., Yan, J., Huang, H., You, Q., and Li, Y. J.: Chromophoric fingerprinting of brown carbon from residential biomass burning, *Environ. Sci. Technol. Lett.*, 9, 102–111, <https://doi.org/10.1021/acs.estlett.1c00837>, 2021.
- Huo, Y., Guo, Z., Li, Q., Wu, D., Ding, X., Liu, A., Huang, D., Qiu, G., Wu, M., Zhao, Z., Sun, H., Song, W., Li, X., Chen, Y., Wu, T., and Chen, J.: Chemical fingerprinting of HULIS in particulate matters emitted from residential coal and biomass combustion, *Environ. Sci. Technol.*, 55, 3593–3603, <https://doi.org/10.1021/acs.est.0c08518>, 2021.
- Jang, K. S., Choi, M., Park, M., Park, M. H., Kim, Y. H., Seo, J., Wang, Y., Hu, M., Bae, M. S., and Park, K.: Assessment of PM<sub>2.5</sub>-bound nitrogen-containing organic compounds (NOCs) during winter at urban sites in China and Korea, *Environ. Pol-*



- lut., 265, 114870, <https://doi.org/10.1016/j.envpol.2020.114870>, 2020.
- Jiang, B., Liang, Y., Xu, C., Zhang, J., Hu, M., and Shi, Q.: Polycyclic aromatic hydrocarbons (PAHs) in ambient aerosols from Beijing: characterization of low volatile PAHs by positive-ion atmospheric pressure photoionization (APPI) coupled with Fourier transform ion cyclotron resonance, *Environ. Sci. Technol.*, 48, 4716–4723, <https://doi.org/10.1021/es405295p>, 2014.
- Jiang, H., Li, J., Chen, D., Tang, J., Cheng, Z., Mo, Y., Su, T., Tian, C., Jiang, B., Liao, Y., and Zhang, G.: Biomass burning organic aerosols significantly influence the light absorption properties of polarity-dependent organic compounds in the Pearl River Delta Region, China, *Environ. Int.*, 144, 106079, <https://doi.org/10.1016/j.envint.2020.106079>, 2020.
- Jiang, H., Li, J., Sun, R., Tian, C., Tang, J., Jiang, B., Liao, Y., Chen, C. E., and Zhang, G.: Molecular dynamics and light absorption properties of atmospheric dissolved organic matter, *Environ. Sci. Technol.*, 55, 10268–10279, <https://doi.org/10.1021/acs.est.1c01770>, 2021.
- Koch, B. P. and Dittmar, T.: From mass to structure: an aromaticity index for high-resolution mass data of natural organic matter, *Rapid. Commun. Mass. Sp.*, 20, 926–932, <https://doi.org/10.1002/rcm.2386>, 2006.
- Kourtchev, I., Fuller, S., Aalto, J., Ruuskanen, T. M., McLeod, M. W., Maenhaut, W., Jones, R., Kulmala, M., and Kalberer, M.: Molecular composition of boreal forest aerosol from Hyytiälä, Finland, using ultrahigh resolution mass spectrometry, *Environ. Sci. Technol.*, 47, 4069–4079, <https://doi.org/10.1021/es3051636>, 2013.
- Kourtchev, I., O'Connor, I. P., Giorio, C., Fuller, S. J., Kristensen, K., Maenhaut, W., Wenger, J. C., Sodeau, J. R., Glasius, M., and Kalberer, M.: Effects of anthropogenic emissions on the molecular composition of urban organic aerosols: An ultrahigh resolution mass spectrometry study, *Atmos. Environ.*, 89, 525–532, <https://doi.org/10.1016/j.atmosenv.2014.02.051>, 2014.
- Kourtchev, I., Godoi, R. H. M., Connors, S., Levine, J. G., Archibald, A. T., Godoi, A. F. L., Paralovo, S. L., Barbosa, C. G. G., Souza, R. A. F., Manzi, A. O., Seco, R., Sjøstedt, S., Park, J.-H., Guenther, A., Kim, S., Smith, J., Martin, S. T., and Kalberer, M.: Molecular composition of organic aerosols in central Amazonia: an ultra-high-resolution mass spectrometry study, *Atmos. Chem. Phys.*, 16, 11899–11913, <https://doi.org/10.5194/acp-16-11899-2016>, 2016.
- Kroll, J. H., Donahue, N. M., Jimenez, J. L., Kessler, S. H., Canagaratna, M. R., Wilson, K. R., Altieri, K. E., Mazzoleni, L. R., Wozniak, A. S., Bluhm, H., Mysak, E. R., Smith, J. D., Kolb, C. E., and Worsnop, D. R.: Carbon oxidation state as a metric for describing the chemistry of atmospheric organic aerosol, *Nat. Chem.*, 3, 133–139, <https://doi.org/10.1038/nchem.948>, 2011.
- Kuang, B. Y., Lin, P., Huang, X. H. H., and Yu, J. Z.: Sources of humic-like substances in the Pearl River Delta, China: positive matrix factorization analysis of PM<sub>2.5</sub> major components and source markers, *Atmos. Chem. Phys.*, 15, 1995–2008, <https://doi.org/10.5194/acp-15-1995-2015>, 2015.
- Laskin, A., Smith, J. S., and Laskin, J.: Molecular characterization of nitrogen-containing organic compounds in biomass burning aerosols using high-resolution mass spectrometry, *Environ. Sci. Technol.*, 43, 3764–3771, <https://doi.org/10.1021/es803456n>, 2009.
- Laskin, J., Laskin, A., and Nizkorodov, S. A.: Mass spectrometry analysis in atmospheric chemistry, *Anal. Chem.*, 90, 166–189, <https://doi.org/10.1021/acs.analchem.7b04249>, 2018.
- Levin, I. and Kromer, B.: The tropospheric <sup>14</sup>CO<sub>2</sub> level in mid-latitudes of the Northern Hemisphere (1959–2003), *Radiocarbon*, 46, 1261–1272, <https://doi.org/10.1017/s0033822200033130>, 2004.
- Levin, I., Kromer, B., and Hammer, S.: Atmospheric  $\Delta^{14}\text{CO}_2$  trend in Western European background air from 2000 to 2012, *Tellus B*, 65, 20092, <https://doi.org/10.3402/tellusb.v65i0.20092>, 2013.
- Li, X., Han, J., Hopke, P. K., Hu, J., Shu, Q., Chang, Q., and Ying, Q.: Quantifying primary and secondary humic-like substances in urban aerosol based on emission source characterization and a source-oriented air quality model, *Atmos. Chem. Phys.*, 19, 2327–2341, <https://doi.org/10.5194/acp-19-2327-2019>, 2019.
- Li, X., Yu, F., Cao, J., Fu, P., Hua, X., Chen, Q., Li, J., Guan, D., Tripathee, L., Chen, Q., and Wang, Y.: Chromophoric dissolved organic carbon cycle and its molecular compositions and optical properties in precipitation in the Guanzhong basin, China, *Sci. Total. Environ.*, 814, 152775, <https://doi.org/10.1016/j.scitotenv.2021.152775>, 2022.
- Lin, P., Rincon, A. G., Kalberer, M., and Yu, J. Z.: Elemental composition of HULIS in the Pearl River Delta Region, China: results inferred from positive and negative electrospray high resolution mass spectrometric data, *Environ. Sci. Technol.*, 46, 7454–7462, <https://doi.org/10.1021/es300285d>, 2012a.
- Lin, P., Yu, J. Z., Engling, G., and Kalberer, M.: Organosulfates in humic-like substance fraction isolated from aerosols at seven locations in East Asia: a study by ultra-high-resolution mass spectrometry, *Environ. Sci. Technol.*, 46, 13118–13127, <https://doi.org/10.1021/es303570v>, 2012b.
- Lin, P., Aiona, P. K., Li, Y., Shiraiwa, M., Laskin, J., Nizkorodov, S. A., and Laskin, A.: Molecular characterization of brown carbon in biomass burning aerosol particles, *Environ. Sci. Technol.*, 50, 11815–11824, <https://doi.org/10.1021/acs.est.6b03024>, 2016.
- Lin, P., Bluvshstein, N., Rudich, Y., Nizkorodov, S. A., Laskin, J., and Laskin, A.: Molecular chemistry of atmospheric brown carbon inferred from a nationwide biomass burning event, *Environ. Sci. Technol.*, 51, 11561–11570, <https://doi.org/10.1021/acs.est.7b02276>, 2017.
- Lin, P., Fleming, L. T., Nizkorodov, S. A., Laskin, J., and Laskin, A.: Comprehensive molecular characterization of atmospheric brown carbon by high resolution mass spectrometry with electrospray and atmospheric pressure photoionization, *Anal. Chem.*, 90, 12493–12502, <https://doi.org/10.1021/acs.analchem.8b02177>, 2018.
- Liu, X., Zhang, Y.-L., Peng, Y., Xu, L., Zhu, C., Cao, F., Zhai, X., Haque, M. M., Yang, C., Chang, Y., Huang, T., Xu, Z., Bao, M., Zhang, W., Fan, M., and Lee, X.: Chemical and optical properties of carbonaceous aerosols in Nanjing, eastern China: regionally transported biomass burning contribution, *Atmos. Chem. Phys.*, 19, 11213–11233, <https://doi.org/10.5194/acp-19-11213-2019>, 2019.
- Ma, L., Li, B., Liu, Y., Sun, X., Fu, D., Sun, S., Thapa, S., Geng, J., Qi, H., Zhang, A., and Tian, C.: Characterization, sources and risk assessment of PM<sub>2.5</sub>-bound polycyclic aromatic hydrocarbons (PAHs) and nitrated PAHs (NPAHs) in Harbin, a

- cold city in Northern China, *J. Clean. Prod.*, 264, 121673, <https://doi.org/10.1016/j.jclepro.2020.121673>, 2020.
- Ma, Y., Cheng, Y., Qiu, X., Cao, G., Fang, Y., Wang, J., Zhu, T., Yu, J., and Hu, D.: Sources and oxidative potential of water-soluble humic-like substances (HULIS<sub>WS</sub>) in fine particulate matter (PM<sub>2.5</sub>) in Beijing, *Atmos. Chem. Phys.*, 18, 5607–5617, <https://doi.org/10.5194/acp-18-5607-2018>, 2018.
- Mo, Y., Li, J., Jiang, B., Su, T., Geng, X., Liu, J., Jiang, H., Shen, C., Ding, P., Zhong, G., Cheng, Z., Liao, Y., Tian, C., Chen, Y., and Zhang, G.: Sources, compositions, and optical properties of humic-like substances in Beijing during the 2014 APEC summit: Results from dual carbon isotope and Fourier-transform ion cyclotron resonance mass spectrometry analyses, *Environ. Pollut.*, 239, 322–331, <https://doi.org/10.1016/j.envpol.2018.04.041>, 2018.
- Mohr, C., Lopez-Hilfiker, F. D., Zotter, P., Prevot, A. S., Xu, L., Ng, N. L., Herndon, S. C., Williams, L. R., Franklin, J. P., Zahniser, M. S., Worsnop, D. R., Knighton, W. B., Aiken, A. C., Gorkowski, K. J., Dubey, M. K., Allan, J. D., and Thornton, J. A.: Contribution of nitrated phenols to wood burning brown carbon light absorption in Deling, United Kingdom during winter time, *Environ. Sci. Technol.*, 47, 6316–6324, <https://doi.org/10.1021/es400683v>, 2013.
- Mutzel, A., Poulain, L., Berndt, T., Iinuma, Y., Rodigast, M., Boge, O., Richters, S., Spindler, G., Sipila, M., Jokinen, T., Kulmala, M., and Herrmann, H.: Highly oxidized multifunctional organic compounds observed in tropospheric particles: a field and laboratory study, *Environ. Sci. Technol.*, 49, 7754–7761, <https://doi.org/10.1021/acs.est.5b00885>, 2015.
- Ning, C., Gao, Y., Zhang, H., Yu, H., Wang, L., Geng, N., Cao, R., and Chen, J.: Molecular characterization of dissolved organic matters in winter atmospheric fine particulate matters (PM<sub>2.5</sub>) from a coastal city of northeast China, *Sci. Total. Environ.*, 689, 312–321, <https://doi.org/10.1016/j.scitotenv.2019.06.418>, 2019.
- Ning, C., Gao, Y., Yu, H., Zhang, H., Geng, N., Cao, R., and Chen, J.: FT-ICR mass spectrometry for molecular characterization of water-insoluble organic compounds in winter atmospheric fine particulate matters, *J. Environ. Sci.*, 111, 51–60, <https://doi.org/10.1016/j.jes.2020.12.017>, 2022.
- Noziere, B., Kalberer, M., Claeys, M., Allan, J., D'Anna, B., Decesari, S., Finessi, E., Glasius, M., Grgic, I., Hamilton, J. F., Hoffmann, T., Iinuma, Y., Jaoui, M., Kahnt, A., Kampf, C. J., Kourtchev, I., Maenhaut, W., Marsden, N., Saarikoski, S., Schnelle-Kreis, J., Surratt, J. D., Szidat, S., Szmigielski, R., and Wisthaler, A.: The molecular identification of organic compounds in the atmosphere: state of the art and challenges, *Chem. Rev.*, 115, 3919–3983, <https://doi.org/10.1021/cr5003485>, 2015.
- O'Brien, R. E., Laskin, A., Laskin, J., Rubitschun, C. L., Surratt, J. D., and Goldstein, A. H.: Molecular characterization of S and N containing organic constituents in ambient aerosols by negative ion mode high-resolution Nanospray desorption electrospray ionization mass spectrometry: CalNex 2010 field study, *J. Geophys. Res.-Atmos.*, 119, 12706–12720, <https://doi.org/10.1002/2014jd021955>, 2014.
- Patriarca, C., Bergquist, J., Sjoberg, P. J. R., Tranvik, L., and Hawkes, J. A.: Online HPLC-ESI-HRMS method for the analysis and comparison of different dissolved organic matter samples, *Environ. Sci. Technol.*, 52, 2091–2099, <https://doi.org/10.1021/acs.est.7b04508>, 2018.
- Pospisilova, V., Lopez-Hilfiker, F. D., Bell, D. M., Haddad, I. E., Mohr, C., Huang, W., Heikkinen, L., Xiao, M., Dommen, J., Prevot, A. S. H., Baltensperger, U., and Slowik, J. G.: On the fate of oxygenated organic molecules in atmospheric aerosol particles, *Sci. Adv.*, 6, eaax8922, <https://doi.org/10.1126/sciadv.aax8922>, 2020.
- Qi, L., Zhang, Z., Wang, X., Deng, F., Zhao, J., and Liu, H.: Molecular characterization of atmospheric particulate organosulfates in a port environment using ultrahigh resolution mass spectrometry: Identification of traffic emissions, *J. Hazard. Mater.*, 419, 126431, <https://doi.org/10.1016/j.jhazmat.2021.126431>, 2021.
- Riva, M., Tomaz, S., Cui, T., Lin, Y.-H., Perraudin, E., Gold, A., Stone, E. A., Villenave, E., and Surratt, J. D.: Evidence for an unrecognized secondary anthropogenic source of organosulfates and sulfonates: gas-phase oxidation of polycyclic aromatic hydrocarbons in the presence of sulfate aerosol, *Environ. Sci. Technol.*, 49, 6654–6664, <https://doi.org/10.1021/acs.est.5b00836>, 2015.
- Shen, H., Zhao, D., Pullinen, I., Kang, S., Vereecken, L., Fuchs, H., Acir, I. H., Tillmann, R., Rohrer, F., Wildt, J., Kiendler-Scharr, A., Wahner, A., and Mentel, T. F.: Highly oxygenated organic nitrates formed from NO<sub>3</sub> radical-initiated oxidation of beta-Pinene, *Environ. Sci. Technol.*, 55, 15658–15671, <https://doi.org/10.1021/acs.est.1c03978>, 2021.
- Siemens, K., Morales, A., He, Q., Li, C., Hettiyadura, A. P. S., Rudich, Y., and Laskin, A.: Molecular analysis of secondary brown carbon produced from the photooxidation of naphthalene, *Environ. Sci. Technol.*, 56, 3340–3353, <https://doi.org/10.1021/acs.est.1c03135>, 2022.
- Song, J., Li, M., Jiang, B., Wei, S., Fan, X., and Peng, P.: Molecular characterization of water-soluble humic like substances in smoke particles emitted from combustion of biomass materials and coal using Ultrahigh-resolution electrospray ionization fourier transform ion cyclotron resonance mass spectrometry, *Environ. Sci. Technol.*, 52, 2575–2585, <https://doi.org/10.1021/acs.est.7b06126>, 2018.
- Song, J., Li, M., Fan, X., Zou, C., Zhu, M., Jiang, B., Yu, Z., Jia, W., Liao, Y., and Peng, P.: Molecular characterization of water- and methanol-soluble organic compounds emitted from residential coal combustion using Ultrahigh-resolution electrospray ionization fourier transform ion cyclotron resonance mass spectrometry, *Environ. Sci. Technol.*, 53, 13607–13617, <https://doi.org/10.1021/acs.est.9b04331>, 2019.
- Song, J., Li, M., Zou, C., Cao, T., Fan, X., Jiang, B., Yu, Z., Jia, W., and Peng, P.: Molecular characterization of nitrogen-containing compounds in humic-like substances emitted from biomass burning and coal combustion, *Environ. Sci. Technol.*, 56, 119–130, <https://doi.org/10.1021/acs.est.1c04451>, 2022.
- Sun, H., Li, X., Zhu, C., Huo, Y., Zhu, Z., Wei, Y., Yao, L., Xiao, H., and Chen, J.: Molecular composition and optical property of humic-like substances (HULIS) in winter-time PM<sub>2.5</sub> in the rural area of North China Plain, *Atmos. Environ.*, 252, 118316, <https://doi.org/10.1016/j.atmosenv.2021.118316>, 2021.
- Surratt, J. D., Gómez-González, Y., Chan, A. W. H., Vermeylen, R., Shahgholi, M., Kleindienst, T. E., Edney, E. O., Offenberg, J. H., Lewandowski, M., Jaoui, M., Maenhaut, W., Claeys, M., Flagan, R. C., and Seinfeld, J. H.: Organosulfate formation in biogenic secondary organic aerosol, *J. Phys. Chem. A*, 112, 8345–8378, <https://doi.org/10.1021/jp802310p>, 2008.

- Tang, J., Li, J., Su, T., Han, Y., Mo, Y., Jiang, H., Cui, M., Jiang, B., Chen, Y., Tang, J., Song, J., Peng, P., and Zhang, G.: Molecular compositions and optical properties of dissolved brown carbon in biomass burning, coal combustion, and vehicle emission aerosols illuminated by excitation–emission matrix spectroscopy and Fourier transform ion cyclotron resonance mass spectrometry analysis, *Atmos. Chem. Phys.*, 20, 2513–2532, <https://doi.org/10.5194/acp-20-2513-2020>, 2020.
- Tao, S., Lu, X., Levac, N., Bateman, A. P., Nguyen, T. B., Bones, D. L., Nizkorodov, S. A., Laskin, J., Laskin, A., and Yang, X.: Molecular characterization of organosulfates in organic aerosols from Shanghai and Los Angeles urban areas by nanospray-desorption electrospray ionization high-resolution mass spectrometry, *Environ. Sci. Technol.*, 48, 10993–11001, <https://doi.org/10.1021/es5024674>, 2014.
- Tsui, W. G. and McNeill, V. F.: Modeling secondary organic aerosol production from photosensitized humic-like substances (HULIS), *Environ. Sci. Technol. Lett.*, 5, 255–259, <https://doi.org/10.1021/acs.estlett.8b00101>, 2018.
- Wang, J., Ge, X., Chen, Y., Shen, Y., Zhang, Q., Sun, Y., Xu, J., Ge, S., Yu, H., and Chen, M.: Highly time-resolved urban aerosol characteristics during springtime in Yangtze River Delta, China: insights from soot particle aerosol mass spectrometry, *Atmos. Chem. Phys.*, 16, 9109–9127, <https://doi.org/10.5194/acp-16-9109-2016>, 2016.
- Wang, J., Zhao, B., Wang, S., Yang, F., Xing, J., Morawska, L., Ding, A., Kulmala, M., Kerminen, V.-M., Kujansuu, J., Wang, Z., Ding, D., Zhang, X., Wang, H., Tian, M., Petäjä, T., Jiang, J., and Hao, J.: Particulate matter pollution over China and the effects of control policies, *Sci. Total Environ.*, 584–585, 426–447, <https://doi.org/10.1016/j.scitotenv.2017.01.027>, 2017.
- Wang, J., Nie, W., Cheng, Y., Shen, Y., Chi, X., Wang, J., Huang, X., Xie, Y., Sun, P., Xu, Z., Qi, X., Su, H., and Ding, A.: Light absorption of brown carbon in eastern China based on 3-year multi-wavelength aerosol optical property observations and an improved absorption Ångström exponent segregation method, *Atmos. Chem. Phys.*, 18, 9061–9074, <https://doi.org/10.5194/acp-18-9061-2018>, 2018.
- Wang, K., Zhang, Y., Huang, R.-J., Cao, J., and Hoffmann, T.: UHPLC-Orbitrap mass spectrometric characterization of organic aerosol from a central European city (Mainz, Germany) and a Chinese megacity (Beijing), *Atmos. Environ.*, 189, 22–29, <https://doi.org/10.1016/j.atmosenv.2018.06.036>, 2018.
- Wang, K., Zhang, Y., Huang, R. J., Wang, M., Ni, H., Kampf, C. J., Cheng, Y., Bilde, M., Glasius, M., and Hoffmann, T.: Molecular characterization and source identification of atmospheric particulate organosulfates using ultrahigh resolution mass spectrometry, *Environ. Sci. Technol.*, 53, 6192–6202, <https://doi.org/10.1021/acs.est.9b02628>, 2019.
- Wang, X., Hayeck, N., Brüggemann, M., Yao, L., Chen, H., Zhang, C., Emmelin, C., Chen, J., George, C., and Wang, L.: Chemical characteristics of organic aerosols in Shanghai: a study by Ultrahigh-performance liquid chromatography coupled with orbitrap mass spectrometry, *J. Geophys. Res.-Atmos.*, 122, 11,703–711,722, <https://doi.org/10.1002/2017jd026930>, 2017.
- Wang, X., Heald, C. L., Liu, J., Weber, R. J., Campuzano-Jost, P., Jimenez, J. L., Schwarz, J. P., and Perring, A. E.: Exploring the observational constraints on the simulation of brown carbon, *Atmos. Chem. Phys.*, 18, 635–653, <https://doi.org/10.5194/acp-18-635-2018>, 2018.
- Wang, X. K., Rossignol, S., Ma, Y., Yao, L., Wang, M. Y., Chen, J. M., George, C., and Wang, L.: Molecular characterization of atmospheric particulate organosulfates in three megacities at the middle and lower reaches of the Yangtze River, *Atmos. Chem. Phys.*, 16, 2285–2298, <https://doi.org/10.5194/acp-16-2285-2016>, 2016.
- Wang, Y., Hu, M., Lin, P., Guo, Q., Wu, Z., Li, M., Zeng, L., Song, Y., Zeng, L., Wu, Y., Guo, S., Huang, X., and He, L.: Molecular characterization of nitrogen-containing organic compounds in humic-like substances emitted from straw residue burning, *Environ. Sci. Technol.*, 51, 5951–5961, <https://doi.org/10.1021/acs.est.7b00248>, 2017.
- Wang, Y., Hu, M., Guo, S., Wang, Y., Zheng, J., Yang, Y., Zhu, W., Tang, R., Li, X., Liu, Y., Le Breton, M., Du, Z., Shang, D., Wu, Y., Wu, Z., Song, Y., Lou, S., Hallquist, M., and Yu, J.: The secondary formation of organosulfates under interactions between biogenic emissions and anthropogenic pollutants in summer in Beijing, *Atmos. Chem. Phys.*, 18, 10693–10713, <https://doi.org/10.5194/acp-18-10693-2018>, 2018.
- Wang, Y., Hu, M., Lin, P., Tan, T., Li, M., Xu, N., Zheng, J., Du, Z., Qin, Y., Wu, Y., Lu, S., Song, Y., Wu, Z., Guo, S., Zeng, L., Huang, X., and He, L.: Enhancement in particulate organic nitrogen and light absorption of humic-like substances over Tibetan Plateau due to long-range transported biomass burning emissions, *Environ. Sci. Technol.*, 53, 14222–14232, <https://doi.org/10.1021/acs.est.9b06152>, 2019.
- Wang, Y., Hu, M., Wang, Y.-C., Li, X., Fang, X., Tang, R., Lu, S., Wu, Y., Guo, S., Wu, Z., Hallquist, M., and Yu, J. Z.: Comparative study of particulate organosulfates in contrasting atmospheric environments: field evidence for the significant influence of anthropogenic sulfate and NO<sub>x</sub>, *Environ. Sci. Technol. Lett.*, 7, 787–794, <https://doi.org/10.1021/acs.estlett.0c00550>, 2020.
- Willoughby, A. S., Wozniak, A. S., and Hatcher, P. G.: A molecular-level approach for characterizing water-insoluble components of ambient organic aerosol particulates using ultrahigh-resolution mass spectrometry, *Atmos. Chem. Phys.*, 14, 10299–10314, <https://doi.org/10.5194/acp-14-10299-2014>, 2014.
- Wozniak, A. S., Bauer, J. E., Sleighter, R. L., Dickhut, R. M., and Hatcher, P. G.: Technical Note: Molecular characterization of aerosol-derived water soluble organic carbon using ultrahigh resolution electrospray ionization Fourier transform ion cyclotron resonance mass spectrometry, *Atmos. Chem. Phys.*, 8, 5099–5111, <https://doi.org/10.5194/acp-8-5099-2008>, 2008.
- Wu, C., Yang, J., Fu, Q., Zhu, B., Ruan, T., and Jiang, G.: Molecular characterization of water-soluble organic compounds in PM<sub>2.5</sub> using ultrahigh resolution mass spectrometry, *Sci. Total. Environ.*, 668, 917–924, <https://doi.org/10.1016/j.scitotenv.2019.03.031>, 2019.
- Wu, G., Ram, K., Fu, P., Wang, W., Zhang, Y., Liu, X., Stone, E. A., Pradhan, B. B., Dangol, P. M., Panday, A. K., Wan, X., Bai, Z., Kang, S., Zhang, Q., and Cong, Z.: Water-soluble brown carbon in atmospheric aerosols from Godavari (Nepal), a regional representative of South Asia, *Environ. Sci. Technol.*, 53, 3471–3479, <https://doi.org/10.1021/acs.est.9b00596>, 2019.
- Xie, M., Chen, X., Hays, M. D., Lewandowski, M., Offenberg, J., Kleindienst, T. E., and Holder, A. L.: Light absorption of secondary organic aerosol: composition and contribution of ni-

- troaromatic compounds, *Environ. Sci. Technol.*, 51, 11607–11616, <https://doi.org/10.1021/acs.est.7b03263>, 2017.
- Xie, X., Chen, Y., Nie, D., Liu, Y., Liu, Y., Lei, R., Zhao, X., Li, H., and Ge, X.: Light-absorbing and fluorescent properties of atmospheric brown carbon: A case study in Nanjing, China, *Chemosphere*, 251, 126350, <https://doi.org/10.1016/j.chemosphere.2020.126350>, 2020.
- Xu, B., Cheng, Z., Gustafsson, Ö., Kawamura, K., Jin, B., Zhu, S., Tang, T., Zhang, B., Li, J., and Zhang, G.: Compound-specific radiocarbon analysis of low molecular weight dicarboxylic acids in ambient aerosols using preparative gas chromatography: method development, *Environ. Sci. Technol. Lett.*, 8, 135–141, <https://doi.org/10.1021/acs.estlett.0c00887>, 2021.
- Yang, Z., Tsona, N. T., Li, J., Wang, S., Xu, L., You, B., and Du, L.: Effects of NO<sub>x</sub> and SO<sub>2</sub> on the secondary organic aerosol formation from the photooxidation of 1,3,5-trimethylbenzene: A new source of organosulfates, *Environ. Pollut.*, 264, 114742, <https://doi.org/10.1016/j.envpol.2020.114742>, 2020.
- Yang, Z., Tsona, N. T., George, C., and Du, L.: Nitrogen-containing compounds enhance Light absorption of aromatic-derived brown carbon, *Environ. Sci. Technol.*, 56, 4005–4016, <https://doi.org/10.1021/acs.est.1c08794>, 2022.
- Zeng, Y., Ning, Y., Shen, Z., Zhang, L., Zhang, T., Lei, Y., Zhang, Q., Li, G., Xu, H., Ho, S. S. H., and Cao, J.: The roles of N, S, and O in molecular absorption features of brown carbon in PM<sub>2.5</sub> in a typical-semi arid megacity in North-western China, *J. Geophys. Res.-Atmos.*, 126, e2021JD034791, <https://doi.org/10.1029/2021jd034791>, 2021.
- Zhang, A., Wang, Y., Zhang, Y., Weber, R. J., Song, Y., Ke, Z., and Zou, Y.: Modeling the global radiative effect of brown carbon: a potentially larger heating source in the tropical free troposphere than black carbon, *Atmos. Chem. Phys.*, 20, 1901–1920, <https://doi.org/10.5194/acp-20-1901-2020>, 2020.
- Zhang, R., Gen, M., Liang, Z., Li, Y. J., and Chan, C. K.: Photochemical reactions of glyoxal during particulate ammonium nitrate photolysis: brown carbon formation, enhanced glyoxal decay, and organic phase formation, *Environ. Sci. Technol.*, 56, 1605–1614, <https://doi.org/10.1021/acs.est.1c07211>, 2022.
- Zhang, T., Shen, Z., Zhang, L., Tang, Z., Zhang, Q., Chen, Q., Lei, Y., Zeng, Y., Xu, H., and Cao, J.: PM<sub>2.5</sub> Humic-like substances over Xi'an, China: Optical properties, chemical functional group, and source identification, *Atmos. Res.*, 234, 104784, <https://doi.org/10.1016/j.atmosres.2019.104784>, 2020.
- Zhang, T., Shen, Z., Zeng, Y., Cheng, C., Wang, D., Zhang, Q., Lei, Y., Zhang, Y., Sun, J., Xu, H., Ho, S. S. H., and Cao, J.: Light absorption properties and molecular profiles of HULIS in PM<sub>2.5</sub> emitted from biomass burning in traditional “Heated Kang” in Northwest China, *Sci. Total. Environ.*, 776, 146014, <https://doi.org/10.1016/j.scitotenv.2021.146014>, 2021.
- Zhang, T., Huang, S., Wang, D., Sun, J., Zhang, Q., Xu, H., Hang Ho, S. S., Cao, J., and Shen, Z.: Seasonal and diurnal variation of PM<sub>2.5</sub> HULIS over Xi'an in Northwest China: Optical properties, chemical functional group, and relationship with reactive oxygen species (ROS), *Atmos. Environ.*, 268, 118782, <https://doi.org/10.1016/j.atmosenv.2021.118782>, 2022a.
- Zhang, T., Shen, Z., Huang, S., Lei, Y., Zeng, Y., Sun, J., Zhang, Q., Ho, S. S. H., Xu, H., and Cao, J.: Optical properties, molecular characterizations, and oxidative potentials of different polarity levels of water-soluble organic matters in winter PM<sub>2.5</sub> in six China's megacities, *Sci. Total. Environ.*, 853, 158600, <https://doi.org/10.1016/j.scitotenv.2022.158600>, 2022b.
- Zhang, Y., Forrister, H., Liu, J., Dibb, J., Anderson, B., Schwarz, J. P., Perring, A. E., Jimenez, J. L., Campuzano-Jost, P., Wang, Y., Nenes, A., and Weber, R. J.: Top-of-atmosphere radiative forcing affected by brown carbon in the upper troposphere, *Nat. Geosci.*, 10, 486–489, <https://doi.org/10.1038/NGEO2960>, 2017.
- Zhao, M., Qiao, T., Li, Y., Tang, X., Xiu, G., and Yu, J. Z.: Temporal variations and source apportionment of Hulis-C in PM<sub>2.5</sub> in urban Shanghai, *Sci. Total. Environ.*, 571, 18–26, <https://doi.org/10.1016/j.scitotenv.2016.07.127>, 2016.
- Zhao, Y., Hallar, A. G., and Mazzoleni, L. R.: Atmospheric organic matter in clouds: exact masses and molecular formula identification using ultrahigh-resolution FT-ICR mass spectrometry, *Atmos. Chem. Phys.*, 13, 12343–12362, <https://doi.org/10.5194/acp-13-12343-2013>, 2013.
- Zheng, G., He, K., Duan, F., Cheng, Y., and Ma, Y.: Measurement of humic-like substances in aerosols: A review, *Environ. Pollut.*, 181, 301–314, <https://doi.org/10.1016/j.envpol.2013.05.055>, 2013.
- Zheng, Y., Chen, Q., Cheng, X., Mohr, C., Cai, J., Huang, W., Shrivastava, M., Ye, P., Fu, P., Shi, X., Ge, Y., Liao, K., Miao, R., Qiu, X., Koenig, T. K., and Chen, S.: Precursors and pathways leading to enhanced secondary organic aerosol formation during severe haze episodes, *Environ. Sci. Technol.*, 55, 15680–15693, <https://doi.org/10.1021/acs.est.1c04255>, 2021.